

# EVM Analysis of Distributed Massive MIMO with 1-Bit Radio-Over-Fiber Fronthaul

Anzhong Hu, *Member, IEEE*, Lise Aabel, Giuseppe Durisi, *Senior Member, IEEE*, Sven Jacobsson, Mikael Coldrey, Christian Fager, *Senior Member, IEEE*, Christoph Studer, *Senior Member, IEEE*

**Abstract**—We analyze the uplink performance of a distributed massive multiple-input multiple-output (MIMO) architecture in which the remotely located access points (APs) are connected to a central processing unit via a fiber-optical fronthaul carrying a dithered and 1-bit quantized version of the received radio-frequency (RF) signal. The innovative feature of the proposed architecture is that no down-conversion is performed at the APs. This eliminates the need to equip the APs with local oscillators, which may be difficult to synchronize. Under the assumption that a constraint is imposed on the amount of data that can be exchanged across the fiber-optical fronthaul, we investigate the tradeoff between spatial oversampling, defined in terms of the total number of APs, and temporal oversampling, defined in terms of the oversampling factor selected at the central processing unit, to facilitate the recovery of the transmitted signal from 1-bit samples of the RF received signal. Using the so-called error-vector magnitude (EVM) as performance metric, we shed light on the optimal design of the dither signal, and quantify, for a given number of APs, the minimum fronthaul rate required for our proposed distributed massive MIMO architecture to outperform a standard co-located massive MIMO architecture in terms of EVM.

**Index Terms**—Bussgang’s theorem, nonsubtractive dithering, error vector magnitude, massive multiple-input multiple-output, orthogonal frequency-division multiplexing, 1-bit analog-to-digital converters.

## I. INTRODUCTION

Distributed massive multiple-input multiple-output (MIMO) (also referred in the literature as cell-free massive MIMO), refers to an architecture, in which a large number of access points (APs) serve, in a coordinated way, a much smaller number of user equipments (UEs) over a given coverage area [2]–[4]. Coordination is provided by a central processing unit (CPU) connected to the APs via fronthaul links. The most effective form of coordination is achieved when the CPU performs all digital processing tasks (including channel estimation and spatial processing) up to digital-to-analog and analog-to-digital conver-

sion, whereas the APs perform only analog processing, including up- and down-conversion [5].

Distributed massive MIMO architectures have been shown to be advantageous over more traditional co-located massive MIMO architectures, where a single base station (BS), equipped with a large number of co-located antennas, serves all users in the coverage area. Indeed, when equipped with linear minimum mean-squared error (LMMSE) spatial filtering and fully-centralized processing, distributed massive MIMO solutions are able to exploit macro-diversity, and can mitigate the path-loss variations experienced in co-located massive MIMO architectures. This results in a more uniform quality of service across the coverage area compared to co-located solutions [5]. To make distributed massive MIMO practical, serial network topologies and distributed algorithms to reduce fronthaul signaling have been recently investigated [6], [7].

*Practical Challenges:* A crucial and often implicit assumption behind the theoretical analyses illustrating the advantages of distributed massive MIMO architectures over co-located architectures is that the APs are able to operate in a phase-coherent way when performing up- and down-conversion of the radio frequency (RF) signals. In practice, however, each AP will need to be equipped with an individual oscillator. This will result in independent phase noise during up- and down-conversion, which, if not compensated for, will affect performance significantly. Synchronizing such oscillators via the distribution of a common clock is challenging even in co-located massive MIMO architectures, especially at millimeter-wave frequencies [8]. Such an approach appears even more challenging in distributed deployments, also at lower frequencies. Hence, transmission resources, in the form of control signals for synchronization purposes, need to be sacrificed to make the system operate coherently. Performing such a synchronization over a large number of APs is, however, a nontrivial task and guaranteeing a low synchronization error may not even be possible in certain distributed MIMO deployments [9].

This issue has recently motivated the exploration of an alternative hardware architecture, in which CPU and APs are connected via a fiber-optical fronthaul, and the independent phase-noise resulting from the use of individual oscillators at the APs is avoided by letting the CPU, instead of the AP, perform up- and down-conversion [10], [11]. Since transferring analog RF signals over a fiber-optical fronthaul is challenging due to the high linearity requirements, the authors of [10], [11], building on results previously reported in [12]–[15], propose to map a dithered version of the RF signal into a two-level square waveform, before transmission over the fronthaul link.

The work of L. Aabel, C. Fager, and G. Durisi was supported in part by the Swedish Foundation for Strategic Research under Grant ID19-0036. This research has also been carried out in part within the Gigahertz-ChaseOn Bridge Center, in a project financed by Chalmers, Ericsson, and Qamcom.

Anzhong Hu is with the School of Communication Engineering, Hangzhou Dianzi University, Hangzhou, China (e-mail: huaz@hdu.edu.cn).

Lise Aabel, Sven Jacobsson and Mikael Coldrey are with Ericsson AB, Gothenburg, Sweden. (e-mail: {lise.aabel,sven.jacobsson,mikael.coldrey}@ericsson.com).

Giuseppe Durisi and Christian Fager are with Chalmers University of Technology, Gothenburg, Sweden (e-mail: {durisi,christian.fager}@chalmers.se).

Christoph Studer is with the Department of Information Technology and Electrical Engineering, ETH Zurich, Zurich, Switzerland (e-mail: studer@ethz.ch).

This paper was presented in part at the IEEE Global Telecommunication Conference (GLOBECOM), Waikoloa, HI, USA, 2019 [1].

Specifically, in the downlink of the architecture proposed and experimentally demonstrated via a testbed in [10], [11], the CPU generates the desired base-band (BB) digital signals and up-converts them into temporally oversampled 1-bit digital RF signals by means of a sigma-delta modulator. The resulting two-level analog signals at the output of the digital-to-analog converters are then transferred to the single-antenna APs via the fiber-optical fronthaul, where they are band-pass (BP) filtered (to remove quantization noise), amplified, and fed to the antenna element.

In the uplink, the received signal at each AP is amplified, filtered, and then converted into a two-level analog signal by means of a comparator, whose second port is connected to a dither signal generated at the CPU and conveyed to the APs via the downlink fiber-optical fronthaul. The resulting signal is sent to the CPU via the uplink fiber-optical fronthaul, where it is sampled and fed to the digital signal processing (DSP) unit. The testbed measurements reported in [10], [11], [16] show that this architecture, which can be implemented using low-cost, off-the-shelf components, and which we shall refer to in the remainder of the paper as *distributed massive MIMO with 1-bit radio-over-fiber fronthaul*, yields satisfactory performance in terms of error vector magnitude (EVM).

The purpose of this paper is twofold: we present a theoretical framework for the analysis of the uplink EVM attainable with the distributed massive MIMO with 1-bit radio-over-fiber fronthaul architecture presented in [10], [11], [16], and use this framework to provide insights into the optimal choice of system parameters such as the power of the dither signal, the required fronthaul capacity, the number of APs, and the oversampling rate (OSR) to be employed at the CPU to reconstruct the RF signal from the two-level waveform transmitted over the fiber-optical fronthaul.

*State of the Art:* The problem of analyzing the performance of co-located massive MIMO architectures in the presence of nonlinearities caused by low-precision converters is well-studied in the literature (see, e.g., [17]–[21]). In this line of work, low-precision quantizers are introduced to limit the power consumption and to alleviate the throughput requirements on the fronthaul links connecting the (single) radio unit to the CPU. The main finding in these papers is that satisfactory performance can be achieved both in the uplink and in the downlink, provided that the number of antennas at the BS is sufficiently large, and that dithering is used to whiten the quantization noise, whenever the signal-to-interference-and-noise ratio is large.

Some of these findings have recently been extended to the distributed massive MIMO setting. Specifically, low-precision quantizers are introduced in this setting to model a constraint on the capacity of the fronthaul links connecting the APs to the CPU, and similar conclusions, in terms of achievable performance, are reached [22]–[26]. However, in these works, a *homodyne* transceiver architecture is assumed, which means that quantization is performed on the real and imaginary parts of the complex-valued BB signal (either before or after spatial processing at the AP), whereas in the present paper we will consider an architecture in which quantization is performed directly on the real-valued RF (i.e., BP) signal and spatial processing is performed entirely at the CPU.

To achieve satisfactory performance with the architecture

proposed in [10], [11], it is imperative that the two-level signal carrying a 1-bit quantized version of the RF signal is sampled at a much higher rate than the one required for the BB signal. The benefits of oversampling in the presence of 1-bit converters have been pointed out previously in the literature (see, e.g., [27], [28]), although only for scenarios in which quantization is performed on the BB signal. Hence, the question whether spatial oversampling obtained via the deployment of multiple APs can mitigate the need for temporal oversampling remains largely unexplored in the literature.

*Contributions:* We consider a distributed multiuser massive MIMO system in which  $U$  UEs are served by  $B$  distributed APs connected to a CPU via a 1-bit radio-over-fiber fronthaul, and characterize the performance, in terms of EVM, achievable in the uplink. Our characterization relies on an application of Bussgang’s decomposition [29] on a frequency-domain version of the RF signal received at each AP. This allows us to express the oversampled 1-bit-quantized discrete-time RF signal at the CPU as a linear function of the transmitted BB signal.

For a given fronthaul-rate constraint, which models the processing speed of the analog-to-digital converters (ADCs) at the CPU, and for the case in which the dither signal is modeled as a Gaussian process, we provide expressions for the EVM achievable using different linear spatial combiners developed on the basis of the Bussgang decomposition, including maximum ratio (MR), zero forcing (ZF), and (quantization-aware) LMMSE combiners. We also provide an analytical characterization of the EVM in the asymptotic limit of large fronthaul rate, and interpret it as the EVM of an equivalent distributed MIMO homodyne architecture. This analytical characterization turns out to provide relevant insights into the optimal design of the dither signal.

Focusing on a scenario in which the UEs transmitted power is inversely proportional to the number of APs, to avoid favoring unfairly deployments with high AP density and encourage energy efficiency,<sup>1</sup> we conduct numerical experiments that confirm the correctness of the insights obtained via the asymptotic analysis, and shed light both on the impact of the fronthaul-rate constraint, and on the tradeoff between temporal and spatial oversampling. Here, temporal oversampling is dictated by the OSR at the CPU, whereas spatial oversampling is dictated by the number of APs deployed in the coverage area.

Our numerical results suggest that, under the transmitted-power normalization considered in the paper, when a single UE is active, an MR/ZF combiner is used, and the fronthaul rate is small, temporal oversampling is preferable to spatial oversampling. Specifically, the available fronthaul rate should be used to acquire, from few APs, a highly oversampled version of the two-level RF signal. For the case of LMMSE combiner, however, one can trade spatial oversampling for temporal oversampling in this regime. As the fronthaul rate increases, spatial oversampling becomes preferable for all three combiners. This is because, in the asymptotic regime of infinitely large fronthaul rate, the EVM decreases monotonically with the number of APs. When multiple users are active, spatial oversampling is more desirable than

<sup>1</sup>More sophisticated models to analyze the energy efficiency of distributed MIMO architectures are available in the literature [24]. However, these models pertain scenarios in which part of the signal processing is performed at the APs, and, hence, are not applicable to the architecture considered in the present paper.

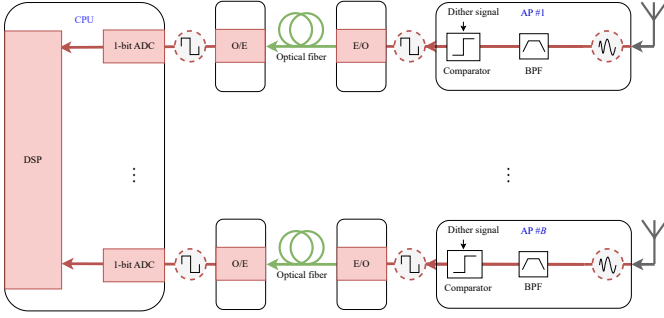


Fig. 1: A distributed massive MIMO uplink architecture consisting of  $B$  APs connected to a CPU via a fiber-optical fronthaul. The received signal at each AP is BP filtered, added to a dither signal and compared with a zero threshold. The resulting two-level signal is converted to the optical domain and transmitted over the optical fiber to the CPU, where it is converted back to the electrical domain, oversampled using a 1-bit ADC, and sent to the DSP for digital down-conversion and spatial processing.

temporal oversampling, even when the fronthaul rate is small, since spatial oversampling reduces multiuser interference.

*Notation:* Lower-case boldface letters are used for vectors and upper-case boldface letters for matrices. We denote by  $\mathcal{CN}(\mathbf{0}_N, \mathbf{R})$  the distribution of an  $N$ -dimensional circularly symmetric complex-valued Gaussian vector with zero mean and  $N \times N$  covariance matrix  $\mathbf{R}$ . We use  $\mathbf{I}_N$  to denote the  $N \times N$  identity matrix,  $\mathbf{0}_N$  to denote the  $N \times 1$  zero vector,  $\mathbf{0}_{N,N}$  to denote  $N \times N$  zero matrix, and  $\mathbb{E}[\cdot]$  and  $\mathbb{P}[\cdot]$  to denote expectation and probability, respectively. For a sequence of random variables  $\{x_n\}$ , we use  $x_n \xrightarrow{\text{a.s.}} x, n \rightarrow \infty$ , where a.s. stands for almost surely, to indicate that  $\mathbb{P}[\lim_{n \rightarrow \infty} x_n = x] = 1$ . The superscripts  $T, *,$  and  $H$  stand for transposition, element-wise conjugation, and Hermitian transposition, respectively. The Kronecker delta function  $\delta[n]$  is defined as  $\delta[0] = 1$  and  $\delta[n] = 0$  for  $n \neq 0$ ,  $\lfloor x \rfloor$  is the largest integer that is smaller or equal to  $x \in \mathbb{R}$ , and  $\text{sgn}(x)$  denotes the sign function, which is equal to  $-1$  if  $x < 0$  and to  $1$  if  $x \geq 0$ . For a matrix  $\mathbf{A}$ , we let  $\text{tr}(\mathbf{A})$  denote its trace and  $\text{diag}(\mathbf{A})$  a diagonal matrix whose diagonal entries coincide with the diagonal entries of  $\mathbf{A}$ . Finally, we use  $[\mathbf{A}]_{b,b'}$  to indicate the entry on row  $b$  and column  $b'$  of  $\mathbf{A}$ .

## II. SYSTEM MODEL

The distributed MIMO architecture considered in this paper and depicted in Fig. 1, follows the structure proposed in [10], [11]. Specifically, the RF signal received at the single-antenna port of  $B$  APs is BP filtered (BPF) and added to a dither signal. The resulting signal is then passed through a zero-threshold comparator, which produces a two-level waveform. This two-level waveform is converted into the optical domain by an electrical-to-optical (E/O) converter and conveyed to the CPU via a fiber-optical fronthaul. At the CPU, the received signal from each AP is converted back to the electrical domain by an optical-to-electrical (O/E) converter, oversampled by a 1-bit ADC, and sent to the DSP for digital down-conversion, spatial processing, and demodulation/decoding.

### A. Signal Parameters and Assumptions

We consider the transmission of a BP signal of bandwidth  $W$  centered at frequency  $f_c \gg W$ .<sup>2</sup> The corresponding received signal at each AP is passed through an ideal BP filter with bandwidth  $W$  centered at  $f_c$  to remove out-of-band noise and interference. We denote by  $f_s$  the sampling frequency of the ADCs at the CPU and focus on the scenario in which  $f_s \gg W$ . Indeed, since we do not perform down-conversion in the analog domain, but only digitally at the CPU, sampling the received signal at the Nyquist rate  $2W$  for the underlying received BB signal may not result in perfect reconstruction, even when no quantization is performed. We will also not necessarily require that  $f_s \geq 2f_c + W$ , since it is possible to reconstruct (again, for the case of no quantization) the underlying BB received signal from samples of the BP signal taken at any rate  $f_s$  satisfying [30]

$$(2f_c + W)/\ell \leq f_s \leq (2f_c - W)/(\ell - 1), \quad (1)$$

where the integer  $\ell$  belongs to the set  $\{1, 2, \dots, \lfloor (f_c + W/2)/W \rfloor\}$ . Note that the choice  $\ell = 1$  results in  $f_s \geq 2f_c + W$ .

Departing from the solution implemented in the testbed described in [10], [11], we shall model, for analytical convenience, the dither signal as a white Gaussian noise process of double-sided spectral density  $E_d/2$  with respect to the bandwidth  $f_s$  (see [31, Def. 25.25.1]).<sup>3</sup>

### B. Discretized Input-Output Relation

For a fixed  $N$ , we focus on the signal received over a time interval of length  $T = N/f_s$ , and write the  $n$ th sample at the output of the  $B$  1-bit ADCs at the CPU as

$$\mathbf{y}_n^{\text{RF}} = \text{sgn}(\mathbf{y}_n^{\text{RF}} + \mathbf{d}_n), \quad n = 0, \dots, N - 1. \quad (2)$$

Here,  $\mathbf{y}_n^{\text{RF}} \in \mathbb{R}^B$  denotes the  $n$ th sample of the discrete-time RF signal before 1-bit quantization but after BP filtering and sampling,  $\mathbf{d}_n \sim \mathcal{N}(\mathbf{0}_B, (E_d/2)\mathbf{I}_B)$  is the Gaussian dither signal (after sampling), which we assume to be independent of  $\mathbf{y}_n^{\text{RF}}$  and independent across  $n$ , and the  $\text{sgn}(\cdot)$  function is applied element-wise to its vector-valued input. We model  $\mathbf{y}_n^{\text{RF}}$  as

$$\mathbf{y}_n^{\text{RF}} = \sqrt{2}\Re\{\mathbf{y}_n^{\text{BB}} e^{j2\pi(f_c/f_s)n}\}, \quad (3)$$

where  $\mathbf{y}_n^{\text{BB}} \in \mathbb{C}^B$  denotes the complex envelope of the discrete-time received signal.

Let now  $S = WT$ , and assume for simplicity that  $S$  is an odd integer. Define the following set:

$$S = \{0, 1, \dots, (S-1)/2, N - (S-1)/2, N - (S-1)/2 + 1, \dots, N - 1\}. \quad (4)$$

<sup>2</sup>For convenience, we shall assume throughout that the ratio  $f_c/W$  is an integer.

<sup>3</sup>In the testbed described in [10], [11], [16], the dither signal is a 17 MHz triangular waveform, generated at the CPU via sigma-delta modulation, and conveyed to the APs via the downlink fronthaul link. As shown in [32], a Gaussian dither signal, which is more difficult to implement, results in slightly better EVM. So our analysis may slightly under-estimate the EVM that would be achievable in practice.



To take into account the correlation introduced on the BB signal  $\mathbf{y}_n^{\text{BB}}$  by oversampling, we shall model it via an inverse discrete Fourier transform as<sup>4</sup>

$$\mathbf{y}_n^{\text{BB}} = \frac{1}{\sqrt{N}} \sum_{k \in \mathcal{S}} (\widehat{\mathbf{H}}_k \hat{\mathbf{s}}_k + \hat{\mathbf{w}}_k) e^{j2\pi \frac{k}{N} n}, \quad (5)$$

where  $\hat{\mathbf{s}}_k \in \mathbb{C}^U$  denotes the discrete signal, expressed in the frequency domain, transmitted by the  $U$  UEs,  $\hat{\mathbf{w}}_k \sim \mathcal{CN}(\mathbf{0}_B, N_0 \mathbf{I}_B)$ ,  $k \in \mathcal{S}$ , denotes the band-limited additive Gaussian noise at the APs, and  $\widehat{\mathbf{H}}_k \in \mathbb{C}^{B \times U}$  denotes the channel frequency response. Throughout, we shall assume that  $\hat{\mathbf{s}}_k \sim \mathcal{CN}(\mathbf{0}_U, E_s \mathbf{I}_U)$ , where  $E_s$  denotes the average energy per sample, and that the vectors  $\{\hat{\mathbf{s}}_k\}_{k \in \mathcal{S}}$  and  $\{\hat{\mathbf{w}}_k\}_{k \in \mathcal{S}}$  are independent, whereas we will allow for arbitrary dependence among the matrices  $\{\widehat{\mathbf{H}}_k\}_{k \in \mathcal{S}}$ . Throughout most of the paper, we shall assume for simplicity that the matrices  $\{\widehat{\mathbf{H}}_k\}_{k \in \mathcal{S}}$  are perfectly known to the CPU.<sup>5</sup> The ratio  $O = N/S = f_s/W$  is the temporal OSR.

### C. Assumptions

We are interested in how the performance of the distributed multiuser massive MIMO architecture with 1-bit radio-over-fiber fronthaul depicted in Fig. 1 is influenced by the number of deployed APs, for a given total coverage area and a given fronthaul rate. To perform a fair comparison between architectures with a different number of APs, we introduce the following two assumptions.

*Fronthaul Constraint:* We assume that there exists a constraint on the number of samples per second that can be processed at the CPU. This imposes a constraint on the total fronthaul rate of the architecture, which we shall denote by  $R_{\text{fh}}$ . Mathematically,  $Bf_s \leq R_{\text{fh}}$ . The following equivalent formulation of the fronthaul constraint will turn out more insightful. For a fixed bandwidth  $W$  of the transmitted signal, we have that

$$BO \leq R_{\text{fh}}/W. \quad (6)$$

In words, according to (6), if we want to deploy more APs, we need to reduce the rate at which the received RF signal at each AP is oversampled.

*Energy-Efficient Setup:* For a fixed coverage area, increasing the number of APs implies reducing the distance between each UE and the closest AP. To benefit from this proximity, without favoring unfairly architectures with a large AP density, and to encourage energy efficiency, we let the transmit power at each UE to be inversely proportional to the number of APs  $B$ . Specifically,

$$E_s = \bar{E}_s/B \quad (7)$$

for a fixed normalized energy per sample  $\bar{E}_s$ . Since we decided to benefit from the APs proximity by reducing the transmit power, we refer to the scenario that results from the assumption (7) as energy-efficient setup.<sup>6</sup>

<sup>4</sup>For simplicity, we shall not consider phase noise or other forms of impairments at the UEs.

<sup>5</sup>The case of imperfect channel knowledge will be discussed in Section V-C.

<sup>6</sup>Under the proposed normalization, and for a uniform two-dimensional AP deployment scenario within a fixed coverage area, the EVM for the case of infinite fronthaul can be shown to converge to a positive value as  $B \rightarrow \infty$ .

### D. Linear Decomposition Using Bussgang's Theorem

Given our assumptions on  $\hat{\mathbf{s}}_k$ ,  $\hat{\mathbf{w}}_k$ , and on the dither signal  $\mathbf{d}_n$ , the input  $\mathbf{q}_n = \mathbf{y}_n^{\text{RF}} + \mathbf{d}_n$  to the quantizer in (2) is a conditionally Gaussian vector given the channel matrices  $\{\widehat{\mathbf{H}}_k\}$ .<sup>7</sup> As a consequence, we can use Bussgang's decomposition [29] to linearize the input-output relation after quantization—an approach that is common in the quantized massive MIMO literature (see, e.g., [18], [34], [33], [21]). Specifically, using Bussgang's decomposition, we can express the quantized signal  $\mathbf{z}_n^{\text{RF}}$  in (2) as

$$\mathbf{z}_n^{\text{RF}} = \mathbf{G}\mathbf{q}_n + \mathbf{e}_n, \quad (8)$$

where  $\mathbf{e}_n \in \mathbb{R}^B$  is the quantization distortion, which is uncorrelated with  $\mathbf{q}_n$ , and  $\mathbf{G} \in \mathbb{R}^{B \times B}$  is the Bussgang gain matrix, given by

$$\mathbf{G} = \sqrt{\frac{2}{\pi}} \text{diag}(\mathbf{R}_{\mathbf{q}}[0])^{-1/2}. \quad (9)$$

Here,  $\mathbf{R}_{\mathbf{q}}[m] = \mathbb{E}[\mathbf{q}_n(\mathbf{q}_{n-m})^T]$  denotes the  $B \times B$  autocovariance matrix of  $\mathbf{q}_n$ . It will turn out important to characterize this quantity for arbitrary values of  $m$ . Since the dither signal is white and independent of the received signal, we conclude that

$$\mathbf{R}_{\mathbf{q}}[m] = \mathbf{R}_{\mathbf{y}^{\text{RF}}}[m] + \frac{E_d}{2} \mathbf{I}_B \delta[m], \quad (10)$$

where  $\mathbf{R}_{\mathbf{y}^{\text{RF}}}[m] = \mathbb{E}[\mathbf{y}_n^{\text{RF}}(\mathbf{y}_{n-m}^{\text{RF}})^T]$ . Furthermore, it follows from (3), (5), and from the fact that the  $\{\hat{\mathbf{s}}_k\}$  and  $\{\hat{\mathbf{w}}_k\}$  are independent and complex proper Gaussian (so that, in particular,  $\mathbb{E}[\hat{\mathbf{s}}_k(\hat{\mathbf{s}}_k)^T] = \mathbf{0}_{U,U}$  and  $\mathbb{E}[\hat{\mathbf{w}}_k(\hat{\mathbf{w}}_k)^T] = \mathbf{0}_{B,B}$  [31, p. 502]), that

$$\mathbf{R}_{\mathbf{y}^{\text{RF}}}[m] = \frac{1}{N} \Re \left\{ \sum_{k \in \mathcal{S}} (E_s \widehat{\mathbf{H}}_k \widehat{\mathbf{H}}_k^H + N_0 \mathbf{I}_B) e^{j2\pi(k/N + f_c/f_s)m} \right\}. \quad (11)$$

Let now  $\mathbf{R}_{\mathbf{e}}[m] = \mathbb{E}[\mathbf{e}_n(\mathbf{e}_{n-m})^T]$  be the autocovariance matrix of the quantization error and  $\mathbf{R}_{\mathbf{z}^{\text{RF}}}[m] = \mathbb{E}[\mathbf{z}_n^{\text{RF}}(\mathbf{z}_{n-m}^{\text{RF}})^T]$  the autocovariance of the quantized signal in (2). It follows from (8) that

$$\mathbf{R}_{\mathbf{e}}[m] = \mathbf{R}_{\mathbf{z}^{\text{RF}}}[m] - \mathbf{G}\mathbf{R}_{\mathbf{q}}[m]\mathbf{G}, \quad (12)$$

where the conditional Gaussianity of  $\mathbf{q}_n$  implies that  $\mathbf{R}_{\mathbf{z}^{\text{RF}}}[m]$  admits the following closed-form expression, usually referred to as arcsine-law [35, Eq. (17)]:

$$\mathbf{R}_{\mathbf{z}^{\text{RF}}}[m] = \frac{2}{\pi} \arcsin\left(\mathbf{D}^{-1/2} \mathbf{R}_{\mathbf{q}}[m] \mathbf{D}^{-1/2}\right). \quad (13)$$

Here,  $\mathbf{D} = \text{diag}(\mathbf{R}_{\mathbf{q}}[0])$ .

### E. Digital Down-Conversion and Linear Combining

To recover the transmitted signal, the CPU down-converts the 1-bit quantized RF signal in the digital domain. Then, it transforms the resulting BB signal into the frequency domain,

<sup>7</sup>It turns out that  $\mathbf{y}_n^{\text{RF}}$  can be well-approximated by a Gaussian random vector also for the case in which the transmitted signal is drawn from commonly used constellations, provided that orthogonal frequency-division multiplexing (OFDM) is used and the number of subcarriers is sufficiently large [33].

and keeps only the frequency samples in the set  $\mathcal{S}$ . This results in

$$\hat{\mathbf{z}}_k^{\text{BB}} = \sqrt{\frac{2}{N}} \sum_{n=0}^{N-1} \mathbf{z}_n^{\text{RF}} e^{-j2\pi(k/N+f_c/f_s)n}, \quad k \in \mathcal{S}. \quad (14)$$

Similarly, let

$$\hat{\mathbf{d}}_k = \sqrt{\frac{2}{N}} \sum_{n=0}^{N-1} \mathbf{d}_n e^{-j2\pi(k/N+f_c/f_s)n} \quad (15)$$

and

$$\hat{\mathbf{e}}_k = \sqrt{\frac{2}{N}} \sum_{n=0}^{N-1} \mathbf{e}_n e^{-j2\pi(k/N+f_c/f_s)n}. \quad (16)$$

It follows from Busssgang's decomposition (8), together with (3), and (5), that

$$\hat{\mathbf{z}}_k^{\text{BB}} = \mathbf{G}(\hat{\mathbf{H}}_k \hat{\mathbf{s}}_k + \hat{\mathbf{w}}_k + \hat{\mathbf{d}}_k) + \hat{\mathbf{e}}_k, \quad k \in \mathcal{S}. \quad (17)$$

It will turn out convenient to characterize the covariance matrix  $\mathbf{C}_{\hat{\mathbf{e}}_k} = \mathbb{E}[\hat{\mathbf{e}}_k(\hat{\mathbf{e}}_k)^H]$ . It follows from (16) that

$$\mathbf{C}_{\hat{\mathbf{e}}_k} = 2 \sum_{m=0}^{N-1} \mathbf{R}_e[m] e^{-j2\pi(k/N+f_c/f_s)m}, \quad (18)$$

where  $\mathbf{R}_e[m]$  can be evaluated in closed form by substituting (10), (11), and (13) into (12).

### III. ANALYSIS OF THE EVM

We assume that the CPU uses its knowledge of the channel  $\hat{\mathbf{H}}_k$ ,  $k \in \mathcal{S}$ , to recover the transmitted signal in the frequency domain,  $\hat{\mathbf{s}}_k$ , via linear combining. Specifically, consider an arbitrary frequency-dependent linear combiner, and denote by  $\mathbf{A}_k \in \mathbb{C}^{U \times B}$ , the combining matrix for the  $k$ th frequency sample. We assume that the CPU obtains an estimate  $\hat{\mathbf{s}}_k^{\text{est}} \in \mathbb{C}^U$  of  $\hat{\mathbf{s}}_k$  as

$$\hat{\mathbf{s}}_k^{\text{est}} = \mathbf{A}_k \hat{\mathbf{z}}_k^{\text{BB}} = \mathbf{A}_k (\mathbf{G}(\hat{\mathbf{H}}_k \hat{\mathbf{s}}_k + \hat{\mathbf{w}}_k + \hat{\mathbf{d}}_k) + \hat{\mathbf{e}}_k). \quad (19)$$

We characterize the quality of the recovered signal in terms of the average EVM  $\eta$ , which we define as<sup>8</sup>

$$\eta = \sqrt{\frac{\sum_{k \in \mathcal{S}} \mathbb{E}[\|\hat{\mathbf{s}}_k^{\text{est}} - \hat{\mathbf{s}}_k\|^2]}{\sum_{k \in \mathcal{S}} \mathbb{E}[\|\hat{\mathbf{s}}_k\|^2]}} = \sqrt{\frac{\sum_{k \in \mathcal{S}} \mathbb{E}[\|\hat{\mathbf{s}}_k^{\text{est}} - \hat{\mathbf{s}}_k\|^2]}{E_s U S}}, \quad (20)$$

where in the last step we used that the entries of  $\hat{\mathbf{s}}_k$  have zero mean and variance  $E_s = \bar{E}_s/B$ .

Clearly, among all possible linear spatial combiners, the Busssgang LMMSE combiner [36]–[38], i.e., the LMMSE combiner based on the Busssgang decomposition (19), minimizes the EVM. However, this combiner may not always be implementable because of complexity constraints, or lack of knowledge of second-order statistics of the channel. Hence, in the remainder of the section, we will also provide expressions for the EVM obtainable using lower-complexity combiners such as the Busssgang MR and Busssgang ZF combiners [39], [38]. The interested reader can find an explicit derivation of all these combiners in, e.g., [38, Sec. II.C].

<sup>8</sup>This quantity is sometimes referred to also as modulation error ratio.

1) *Busssgang MR Combiner*: We assume that the CPU uses a Busssgang MR combiner. Specifically, in view of (19), we set<sup>9</sup>

$$\mathbf{A}_k = \mathbf{E}_k \mathbf{G}^{-1}, \quad (21)$$

where<sup>10</sup>

$$\mathbf{E}_k = \text{diag}(\hat{\mathbf{H}}_k^H \hat{\mathbf{H}}_k)^{-1} \hat{\mathbf{H}}_k^H. \quad (22)$$

Let now

$$\mathbf{B}_k = \text{diag}(\hat{\mathbf{H}}_k^H \hat{\mathbf{H}}_k)^{-1} (\hat{\mathbf{H}}_k^H \hat{\mathbf{H}}_k - \text{diag}(\hat{\mathbf{H}}_k^H \hat{\mathbf{H}}_k)). \quad (23)$$

Then, the estimated sample at the CPU after linear combining can be expressed as

$$\hat{\mathbf{s}}_k^{\text{est}} = \hat{\mathbf{s}}_k + \mathbf{B}_k \hat{\mathbf{s}}_k + \mathbf{E}_k (\hat{\mathbf{w}}_k + \hat{\mathbf{d}}_k) + \mathbf{E}_k \mathbf{G}^{-1} \hat{\mathbf{e}}_k. \quad (24)$$

Substituting (24) into (20), and using that  $\hat{\mathbf{e}}_k$  is uncorrelated with all other quantities, we obtain

$$\eta^2 = \frac{1}{E_s U S} \sum_{k \in \mathcal{S}} \left( E_s \mathbb{E}[\text{tr}(\mathbf{B}_k \mathbf{B}_k^H)] + (N_0 + E_d) \mathbb{E}[\text{tr}(\mathbf{E}_k \mathbf{E}_k^H)] \right) \quad (25)$$

$$+ \mathbb{E}[\text{tr}(\mathbf{E}_k \mathbf{G}^{-1} \mathbf{C}_{\hat{\mathbf{e}}_k} \mathbf{G}^{-1} \mathbf{E}_k^H)]. \quad (26)$$

2) *Busssgang ZF Combiner*: We consider now the case in which a Busssgang ZF combiner is used. Specifically, we assume that

$$\mathbf{A}_k = \mathbf{F}_k \mathbf{G}^{-1}, \quad (27)$$

where

$$\mathbf{F}_k = (\hat{\mathbf{H}}_k^H \hat{\mathbf{H}}_k)^{-1} \hat{\mathbf{H}}_k^H. \quad (28)$$

Then the sample estimate  $\hat{\mathbf{s}}_k^{\text{est}}$  at the CPU after linear combining can be expressed as

$$\hat{\mathbf{s}}_k^{\text{est}} = \hat{\mathbf{s}}_k + \mathbf{F}_k (\hat{\mathbf{w}}_k + \hat{\mathbf{d}}_k) + \mathbf{F}_k \mathbf{G}^{-1} \hat{\mathbf{e}}_k. \quad (29)$$

Substituting (29) into (20), and using again that  $\hat{\mathbf{e}}_k$  is uncorrelated with all other quantities, we obtain

$$\eta^2 = \frac{1}{E_s U S} \sum_{k \in \mathcal{S}} \left( (N_0 + E_d) \mathbb{E}[\text{tr}(\mathbf{F}_k \mathbf{F}_k^H)] + \mathbb{E}[\text{tr}(\mathbf{F}_k \mathbf{G}^{-1} \mathbf{C}_{\hat{\mathbf{e}}_k} \mathbf{G}^{-1} \mathbf{F}_k^H)] \right). \quad (30)$$

3) *Busssgang LMMSE Combiner*: Finally, we consider the Busssgang LMMSE combiner

$$\mathbf{A}_k = \hat{\mathbf{H}}_k^H \left( \hat{\mathbf{H}}_k \hat{\mathbf{H}}_k^H + \frac{N_0 + E_d}{E_s} \mathbf{I}_B + \frac{1}{E_s} \mathbf{G}^{-1} \mathbf{C}_{\hat{\mathbf{e}}_k} \mathbf{G}^{-1} \right)^{-1} \mathbf{G}^{-1} \quad (31)$$

<sup>9</sup>In the remainder of the paper, the index  $k$  is always assumed to belong to the set  $\mathcal{S}$ , although this may not be explicitly mentioned.

<sup>10</sup>The expression for the combiners in (21) and (27) include an array-gain normalization factor.

which, as already mentioned, minimizes the EVM in (20) and results in

$$\begin{aligned} & \mathbb{E} [\|\hat{\mathbf{s}}_k^{\text{est}} - \hat{\mathbf{s}}_k\|^2] \\ &= \text{tr} \left( \mathbb{E} [\hat{\mathbf{s}}_k \hat{\mathbf{s}}_k^H] \right. \\ & \quad \left. - \mathbb{E} [\hat{\mathbf{s}}_k (\hat{\mathbf{z}}_k^{\text{BB}})^H] \mathbb{E} [\hat{\mathbf{z}}_k^{\text{BB}} (\hat{\mathbf{z}}_k^{\text{BB}})^H]^{-1} \mathbb{E} [\hat{\mathbf{z}}_k^{\text{BB}} \hat{\mathbf{s}}_k^H] \right) \quad (32) \\ &= E_s U \\ & \quad - \text{tr} \left( E_s^2 \mathbb{E} \left[ \hat{\mathbf{H}}_k^H \left( E_s \hat{\mathbf{H}}_k \hat{\mathbf{H}}_k^H \right. \right. \right. \\ & \quad \left. \left. \left. + (N_0 + E_d) \mathbf{I}_B + \mathbf{G}^{-1} \mathbf{C}_{\hat{\mathbf{e}}_k} \mathbf{G}^{-1} \right)^{-1} \hat{\mathbf{H}}_k \right] \right). \quad (33) \end{aligned}$$

Let now

$$\mathbf{Z}_k = \hat{\mathbf{H}}_k^H \left( \frac{N_0 + E_d}{E_s} \mathbf{I}_B + \frac{1}{E_s} \mathbf{G}^{-1} \mathbf{C}_{\hat{\mathbf{e}}_k} \mathbf{G}^{-1} \right)^{-1} \hat{\mathbf{H}}_k. \quad (34)$$

Substituting (33) into (20) and using the matrix inversion lemma [40, Sec. 0.7.4], we obtain

$$\eta^2 = 1 - \frac{1}{US} \sum_{k \in \mathcal{S}} \text{tr} (\mathbb{E} [\mathbf{Z}_k - \mathbf{Z}_k (\mathbf{I}_U + \mathbf{Z}_k)^{-1} \mathbf{Z}_k]) \quad (35)$$

$$= \frac{1}{US} \sum_{k \in \mathcal{S}} \text{tr} (\mathbb{E} [(\mathbf{I}_U + \mathbf{Z}_k)^{-1}]). \quad (36)$$

Please note that the expectations in (26), (30), and (36) are only with respect to the distribution of the fading channels. The expectations with respect to the input symbols, the dither signal, and the additive noise are evaluated in closed form.

We provide next insights on the tradeoff between OSR and number of APs, for a given fronthaul constraint, and on the impact of the fronthaul constraint on performance by focusing on the special case of flat-fading channel and considering the asymptotic limit  $N \rightarrow \infty$ .

#### IV. ASYMPTOTIC CHARACTERIZATION OF THE EVM

We now provide an asymptotic characterization of the EVM for the case in which the channel between each UE and AP is frequency flat, i.e.,  $\hat{\mathbf{H}}_k = \mathbf{H}$  for all  $k \in \mathcal{S}$ . Specifically, for a fixed transmitted-signal bandwidth  $W$ , and a fixed number of APs  $B$ , we consider the asymptotic regime in which the sampling rate  $f_s$  goes to infinity. This is equivalent to assuming that the number of samples  $N = T f_s$  over the observation interval  $T$ , the OSR  $O = N/S$  (where  $S = WT$ ), and the fronthaul rate  $R_{\text{fh}} = B f_s$  all go to infinity. Our main finding is that, in this asymptotic limit, the Bussgang gain matrix  $\mathbf{G}$  and the covariance matrix  $\mathbf{C}_{\hat{\mathbf{e}}_k}$  of the quantization error both converge to a scaled identity matrix, provided that  $E_d > 0$ . This allows us to replace (17) with an equivalent input-output relation in which the total additive noise is uncorrelated. As we shall show, this equivalent input-output relation can be interpreted as the one of a conventional distributed MIMO system, in which the CPU has access to infinite-precision samples of the BB signal received at each AP.

#### A. The Matrices $\mathbf{G}$ and $\mathbf{C}_{\hat{\mathbf{e}}_k}$ in the Frequency-Flat Fading Case, and their Asymptotic Limit

Assume that  $\hat{\mathbf{H}}_k = \mathbf{H}$  for all  $k \in \mathcal{S}$  (frequency-flat fading assumption) and let  $\mathbf{h}_b^T$  denote the  $b$ th row of  $\mathbf{H}$ . Let us also introduce the following quantities:

$$p_b = \sqrt{\frac{S}{N} (E_s \|\mathbf{h}_b\|^2 + N_0) + \frac{E_d}{2}}, \quad b = 1, \dots, B, \quad (37)$$

$$c[m] = \sum_{k \in \mathcal{S}} e^{-j2\pi \frac{k}{N} m} = 1 + 2 \sum_{k=1}^{(S-1)/2} \cos(2\pi(mk)/N), \quad (38)$$

where the last equality in (38) follows from (4) and because  $S$  is odd. Furthermore, let

$$v_{bb'}[m] = \Re \left\{ (E_s \mathbf{h}_b^T \mathbf{h}_{b'}^* + N_0) e^{j2\pi \frac{f_c}{f_s} m} \right\} \quad (39)$$

$$s_{bb'}[m] = \frac{c[m] v_{bb'}[m] + \frac{E_d}{2} \delta[m] \delta[b - b']}{p_b p_{b'}} \quad (40)$$

and

$$r_{bb'}[m] = \arcsin(s_{bb'}[m]) - s_{bb'}[m], \quad (41)$$

where the last three quantities are defined for all  $b \in \{1, \dots, B\}$ ,  $b' \in \{1, \dots, B\}$ . As a consequence of (9), (10), and (11), we can express the entry in position  $(b, b)$  of the diagonal matrix  $\mathbf{G}$  as

$$[\mathbf{G}]_{b,b} = \sqrt{\frac{2}{\pi}} \frac{1}{p_b}. \quad (42)$$

Furthermore, it follows from (18), (12), (11), and (13) that the entry in position  $(b, b')$  of the matrix  $\mathbf{C}_{\hat{\mathbf{e}}_k}$  can be expressed as

$$[\mathbf{C}_{\hat{\mathbf{e}}_k}]_{b,b'} = \frac{4}{\pi} \sum_{m=0}^{N-1} r_{bb'}[m] e^{-j2\pi(k/N + f_c/f_s)m}. \quad (43)$$

We are interested in determining the asymptotic behavior of the matrices  $\mathbf{G}$  and  $\mathbf{C}_{\hat{\mathbf{e}}_k}$  in the asymptotic limit  $N \rightarrow \infty$ . It follows immediately from (42) that, whenever  $E_d > 0$ ,

$$[\mathbf{G}]_{b,b} \xrightarrow{\text{a.s.}} \sqrt{\frac{4}{\pi E_d}}, \quad N \rightarrow \infty. \quad (44)$$

To establish a similar result for  $\mathbf{C}_{\hat{\mathbf{e}}_k}$ , we provide in the following lemma a characterization of the asymptotic behavior of  $r_{bb'}[m]$  in (41).

*Lemma 1:* The random variable  $r_{bb'}[m]$  in (41) satisfies the following properties:

$$r_{bb'}[m] \leq r_{bb}[0] = \frac{\pi}{2} - 1 \quad (45)$$

and, for  $b \neq b'$  or  $m \neq 0$

$$|r_{bb'}[m]| \xrightarrow{\text{a.s.}} 0, \quad N \rightarrow \infty. \quad (46)$$

Furthermore, for all  $b, b'$ ,

$$\sum_{m=1}^{N-1} |r_{bb'}[m]| \xrightarrow{\text{a.s.}} 0, \quad N \rightarrow \infty. \quad (47)$$

*Proof:* See Appendix A. ■

It now follows from Lemma 1 and (43) that

$$[\mathbf{C}_{\hat{\mathbf{e}}_k}]_{b,b'} \xrightarrow{\text{a.s.}} 2 \left( 1 - \frac{2}{\pi} \right) \delta[b - b'], \quad N \rightarrow \infty. \quad (48)$$

As a consequence,

$$\mathbf{C}_{\hat{\mathbf{e}}_k} \xrightarrow{\text{a.s.}} 2 \left(1 - \frac{2}{\pi}\right) \mathbf{I}_B, \quad N \rightarrow \infty. \quad (49)$$

Intuitively speaking, (44) and (49), imply that, in the limit  $N \rightarrow \infty$ , we can replace the BB input-output relation (17) with the following input-output relation

$$\hat{\mathbf{z}}_k^{\text{BB}} = \hat{\mathbf{H}}_k \hat{\mathbf{s}}_k + \tilde{\mathbf{w}}_k, \quad k \in \mathcal{S}, \quad (50)$$

where the noise  $\tilde{\mathbf{w}}_k$ , which is uncorrelated with  $\hat{\mathbf{s}}_k$ , has uncorrelated entries. Specifically,  $\mathbb{E}[\tilde{\mathbf{w}}_k \tilde{\mathbf{w}}_k^H] = (N_0 + \frac{\pi}{2} E_d) \mathbf{I}_B$ . Note that the asymptotically equivalent input-output relation (50) coincides with that of a conventional distributed MIMO architecture, where down-conversion and sampling are performed at the AP, and the (infinite-precision) samples of the BB signal are conveyed to the CPU for digital processing.

The asymptotic limits (44) and (49) cannot be directly used in (26), (30), and (36) to obtain asymptotic expressions for the EVM  $\eta$  in the limit  $N \rightarrow \infty$ . Indeed, one needs to first verify that the expectations in (26), (30), and (36) and the limit  $N \rightarrow \infty$  can be interchanged. This is typically possible under mild assumptions on the fading distribution. Since the exact conditions under which the interchange is possible are typically cumbersome to derive, we provide them in the next theorem only for the case  $U = 1$ , for which the matrix  $\mathbf{H}$  reduces to the  $B$ -dimensional vector  $\mathbf{h}$ . Similar conditions can be established for the case  $U > 1$ .

**Theorem 2:** Let  $f(x) = \arcsin(x) - x$  and  $\gamma_b = \sqrt{S(E_s |h_b|^2 + N_0) + \frac{E_d}{2}}$ . For every fading channel distribution satisfying the technical conditions

$$\sum_{b=1}^B \sum_{b'=1}^B \mathbb{E} \left[ \frac{h_b^* h_{b'}}{\|\mathbf{h}\|^4} \gamma_b \gamma_{b'} \right] < \infty \quad (51)$$

and

$$\sum_{b=1}^B \sum_{b'=1}^B \mathbb{E} \left[ \frac{h_b^* h_{b'}}{\|\mathbf{h}\|^4} \gamma_b \gamma_{b'} \left( \frac{2SE_s |h_b| |h_{b'}| + N_0}{E_d} \right) \right] < \infty, \quad (52)$$

the EVM  $\eta$  with Bussgang MR/ZF combining for the case  $U = 1$  admits the following asymptotic characterization:

$$\lim_{N \rightarrow \infty} \eta^2 = \frac{N_0 + (\pi/2)E_d}{E_s} \mathbb{E} \left[ \frac{1}{\|\mathbf{h}\|^2} \right]. \quad (53)$$

Furthermore, let

$$t_{bb'} = \left( \frac{\pi}{2} - 1 \right) \gamma_b \gamma_{b'} \quad (54)$$

and

$$\bar{t}_{bb'} = \left( \frac{\pi}{2} - 1 \right) S \gamma_b \gamma_{b'} \left( \frac{2SE_s |h_b| |h_{b'}| + N_0}{E_d} \right). \quad (55)$$

For every channel law satisfying the technical condition

$$\mathbb{E} \left[ \frac{1}{1 + \bar{\gamma}} \right] < \infty, \quad (56)$$

where

$$\bar{\gamma} = \|\mathbf{h}\|^2 \left( \sum_{b=1}^B \gamma_b^2 \left( \frac{\pi}{2} - 1 \right) + \frac{2}{E_s} \sum_{b=1}^B \sum_{b'=1}^B t_{bb'} + \frac{2}{E_s S} \sum_{b=1}^B \sum_{b'=1}^B \bar{t}_{bb'} \right)^{-1}, \quad (57)$$

the EVM with Bussgang LMMSE combining admits the following asymptotic characterization:

$$\lim_{N \rightarrow \infty} \eta^2 = \mathbb{E} \left[ \left( 1 + \frac{E_s}{N_0 + (\pi/2)E_d} \|\mathbf{h}\|^2 \right)^{-1} \right]. \quad (58)$$

*Proof:* See Appendix B. ■

### B. Insights from the Asymptotic EVM Characterization

Some remarks on Theorem 2 are in order. The EVM expressions (53) and (58) illustrate that, for a given  $E_d > 0$ , the in-band interference caused by the nonsubtractive, wideband dither signal causes a deterioration of the SNR of the equivalent conventional distributed MIMO architecture from  $E_s/N_0$  to  $E_s/(N_0 + (\pi/2)E_d)$ . The term  $\pi/2$  stems from our assumption that, as  $N$  grows, the bandwidth of the dither signal increases, and is fundamental in wideband-regime analyses of 1-bit quantization systems (see, e.g., [41]).

It is worth noting, though, that (53) and (58) hold for every  $E_d > 0$ . This implies that the asymptotic EVM with Bussgang MR/ZF can be made arbitrarily close to

$$\frac{N_0}{E_s} \mathbb{E} \left[ \frac{1}{\|\mathbf{h}\|^2} \right]. \quad (59)$$

Similarly, the asymptotic EVM with Bussgang LMMSE can be made arbitrarily close to

$$\mathbb{E} \left[ \left( 1 + \frac{E_s}{N_0} \|\mathbf{h}\|^2 \right)^{-1} \right]. \quad (60)$$

Note that (59) and (60) are the squared EVM values achievable with MR/ZF and LMMSE combiners, respectively, in a conventional homodyne distributed MIMO architecture, with infinite precision converters. In other words, if we allow for  $N$  to be sufficiently large, and we set  $E_d$  sufficiently small, the nonlinear distortion caused by the 1-bit quantization in the architecture depicted in Fig. 1, has no impact on performance.

The proofs of Lemma 1 and Theorem 2 provide also relevant insights into the optimal choice of  $E_d$  for the practically relevant case of finite  $N$ , and shed light on the dependence of  $E_d$  on system parameters such as the fronthaul rate, the number of APs, and the type of combiner used at the CPU.

Indeed, note that the results reported in Lemma 1, and, hence, also (49), hold also if we fix  $N$  and let  $E_d \rightarrow \infty$ . This implies that, for every fixed  $N$ , we can whiten the correlation matrix  $\mathbf{C}_{\hat{\mathbf{e}}_k}$  of the quantization error, simply by increasing  $E_d$ . This, however, causes an increase of the in-band interference caused by the dither signal, which, for sufficiently large  $N$ , yields the  $(\pi/2)E_d$  penalty term in (53) and (58). So for a finite  $N$ , we expect that there will be a tension between increasing  $E_d$  to whiten the quantization noise, and reducing  $E_d$  to limit in-band interference.

Some insights into this tension can be obtained by analyzing the term  $p_b$  in (37). For the quantization noise to whiten, we need that  $p_b^2 \approx E_d/2$  for all  $b = 1, \dots, B$ , which occurs whenever

$$\frac{E_d}{2N_0} \gg \frac{S}{N} \left( \frac{E_s}{N_0} |h_b|^2 + 1 \right). \quad (61)$$

At the same time, we would like to minimize  $E_d$ , to reduce the impact of in-band interference caused by the dither signal. We see from (61) that the higher the OSR  $N/S$  or, equivalently, the higher the fronthaul rate  $R_{fh}$ , for a fixed number of APs  $B$ , the smaller the value of  $E_d$  necessary for (61) to hold. The dependence of  $E_d$  on  $B$  for a fixed OSR  $N/S$  is more intricate. On the one hand, the larger  $B$ , the smaller  $E_s$  for a fixed normalized energy  $\bar{E}_s$ , because of the energy-efficient assumption (7). This implies that a smaller  $E_d$  is needed to satisfy (61) for a fixed  $|h_b|^2$ . On the other hand, the larger  $B$ , the smaller the distance between each UE and the closest AP, which results in a higher average  $|h_b|^2$  for that AP. This, in turn, results in a larger  $E_d$  to satisfy (61). Also, how much the left-hand-side of (61) should exceed the right-hand side of (61) depends on the combiner used at the CPU. We expect that Busgang LMMSE will be, in general, less sensitive to  $E_d$ , because it exploits the knowledge of the covariance matrix of the quantization noise. Note that, although we focused this discussion on the case  $U = 1$ , the insights we have just reported hold for arbitrary  $U$ , since they rely on the convergence result (49), which we have established for arbitrary  $U$ .

## V. NUMERICAL INVESTIGATIONS

### A. Single UE

1) *Scenario*: Throughout this subsection, we focus on the case  $U = 1$  and investigate the impact on the EVM of the fronthaul constraint (6), the number of APs deployed within a given coverage area, and the energy of the dither signal.

We consider the scenario depicted in Fig. 2a: a rectangular area of size  $L_r \times W_r$  is covered uniformly by  $B = A^2$  APs, with  $A$  chosen to be an even number. The UE is placed at the center of the coverage area. In the remainder of the paper, we will assume that  $L_r = W_r = 100$  m. We also assume that the APs are at height of 10 m and that the UE is at height of 0 m. Furthermore, the  $B$ -dimensional (frequency-flat) channel vector  $\mathbf{h}$ , whose entries describe the random propagation channel between the UE and each AP, is assumed to follow a  $\mathcal{CN}(\mathbf{0}_B, \mathbf{L})$  distribution, where the diagonal matrix  $\mathbf{L}$  contains on its diagonal the path-loss coefficients between the UE and each AP. The path-loss coefficient, measured in dB, between the UE and the  $b$ th AP is modeled as

$$10 \log_{10}[\mathbf{L}]_{b,b} = -37.6 \log_{10}(d_b/d_0) - 35.3, \quad (62)$$

where  $d_b$  is the distance in meters between the UE and the  $b$ th AP, and  $d_0 = 1$  m. In this section, we shall also consider a noise spectral density  $N_0$  that results in a noise power of  $-94$  dBm and a normalized energy per sample  $\bar{E}_s$ , defined in (7), of 20 dBm. We also set  $f_c = 2.4$  GHz,  $W = 24$  MHz, and  $S = 9$ , and assume a frequency-flat fading.

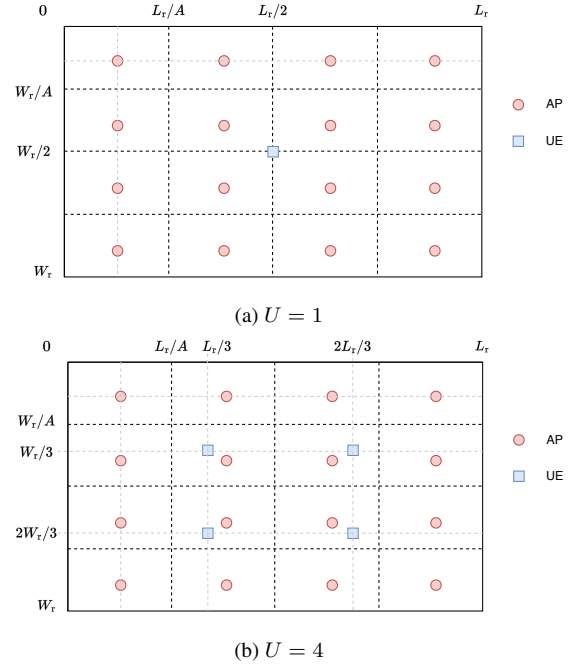


Fig. 2: The topology of the distributed MIMO system for the case  $U = 1$  and  $U = 4$  and fixed UE positions considered in this section. In the two figures,  $B = 16$ .

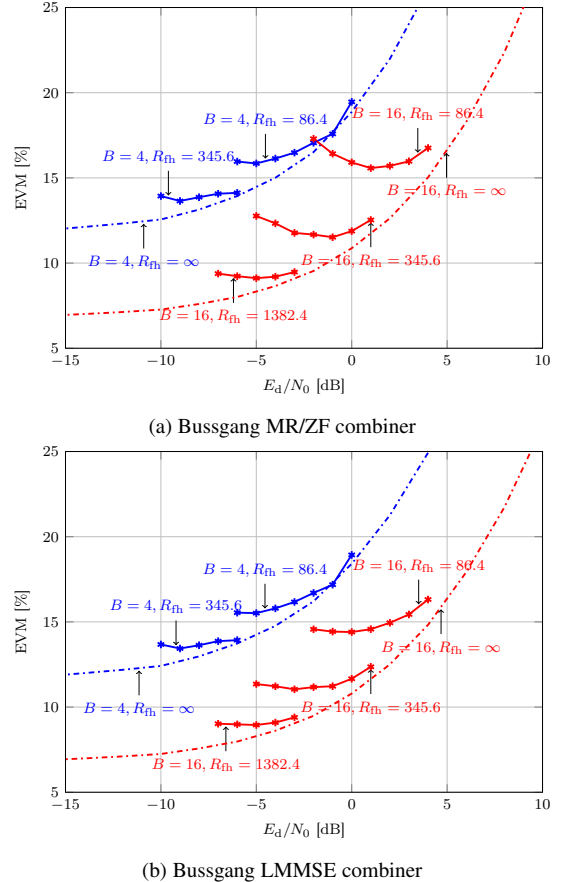


Fig. 3: EVM as a function of the dither-to-noise ratio  $E_d/N_0$ , for the case of Busgang MR/ZF and LMMSE combiners and  $U = 1$ . The values of  $R_{fh}$  are given in Gbit/s. The dot-dashed lines denote the EVM for the case of infinite fronthaul rate, computed using (53) and (58), respectively.

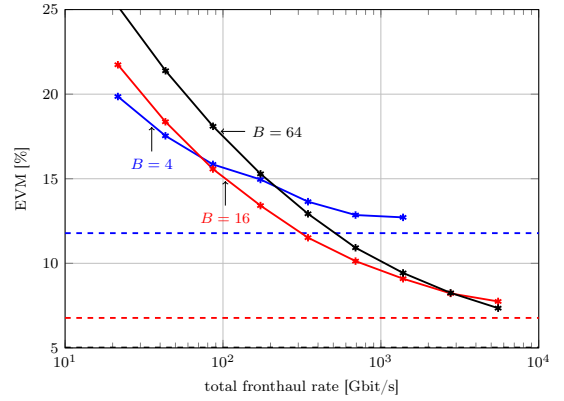


2) *Impact of Dithering*: To validate the insights reported in Section IV-B, based on the asymptotic limit  $N \rightarrow \infty$ , we evaluate in this section the impact of the dither-to-noise ratio  $E_d/N_0$  on the EVM. In Fig. 3, we report the EVM as a function of  $E_d/N_0$  for  $B \in \{4, 16\}$  and  $R_{\text{fh}} \in \{86.4 \text{ Gbit/s}, 345.6 \text{ Gbit/s}, 1382.4 \text{ Gbit/s}\}$  for both Bussgang MR/ZF combiner and LMMSE combiner, computed using the exact nonasymptotic EVM expressions in (26) and (36), as well as the asymptotic ( $R_{\text{fh}} \rightarrow \infty$ ) EVM value, computed using (53) and (58).<sup>11</sup> It is worth mentioning that the testbed designed in [10], [11] involves a CPU that can be connected to up to 12 APs and is equipped with 1-bit ADCs operating at 10 GS/s. This yields a total fronthaul rate of 120 Gbit/s, which is within the range of fronthaul-rate values considered in this section.

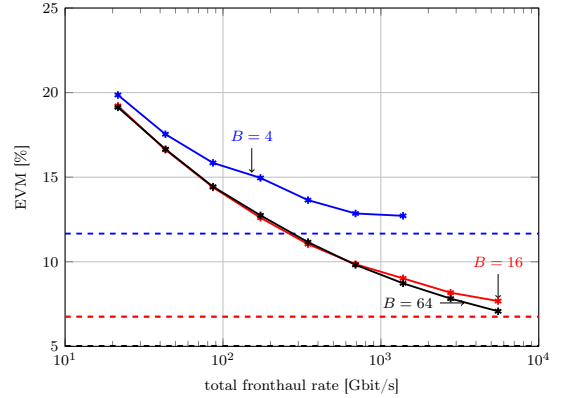
In agreement with our predictions in Section IV-B, for each fixed  $B$  and  $R_{\text{fh}}$ , there exists an optimal non-zero  $E_d/N_0$  value that minimizes the EVM. Operating at a  $E_d/N_0$  larger than the optimal one, allows us to approach the asymptotic EVM predicted by (53) and (58) for that  $E_d/N_0$  value, at the cost of an EVM penalty. We also observe that, as predicted in Section IV-B, for a fixed  $B$ , a larger  $R_{\text{fh}}$  results in a smaller  $E_d/N_0$ . To determine the dependence of  $E_d/N_0$  on  $B$  for a fixed OSR  $O = R_{\text{fh}}/(BW)$ , we compare the curves corresponding to  $B = 4, R_{\text{fh}} = 86.4 \text{ Gbit/s}$  with the curve corresponding to  $B = 16, R_{\text{fh}} = 354.6 \text{ Gbit/s}$ , since, in both cases,  $O = 900$ . We can also compare the curve corresponding to  $B = 4, R_{\text{fh}} = 345.6 \text{ Gbit/s}$  with the curve corresponding to  $B = 16, R_{\text{fh}} = 1382.4 \text{ Gbit/s}$ , since, in both cases  $O = 3600$ . It turns out that in both scenarios, the optimal  $E_d/N_0$  increases when we increase  $B$  for a fixed  $O$ . This suggests that the increase in  $E_d/N_0$  caused by the reduction of the distance between UE and closest AP dominates over the reduction in  $E_d/N_0$  enabled by the lower transmitted power (see (7)). Finally, by comparing Fig. 3a with Fig. 3b, we note, again in agreement with the observations in Section IV-B, that the value of  $E_d/N_0$  that minimizes the EVM is lower when the Bussgang LMMSE combiner is used.

3) *Impact of Fronthaul Rate*: Still focusing on the case  $U = 1$ , in Fig. 4, we illustrate the dependence of the EVM on the fronthaul rate  $R_{\text{fh}}$  for the case of Bussgang MR/ZF combiner and Bussgang LMMSE combiner, computed using (26) and (36) (the value of  $E_d$  is optimized for each value of fronthaul rate considered in the figure), and compare the resulting nonasymptotic EVM with the asymptotic values in (53) and (58), computed by setting  $E_d = 0$ , in accordance to the discussion in Section IV-B.<sup>12</sup> For the case of MR/ZF combiner, we see that, for small values of  $R_{\text{fh}}$ , increasing the number of APs is deleterious in terms of EVM, and the smallest EVM is achieved when  $B = 4$ . This suggests that, when  $R_{\text{fh}}$  is small, it is better to use the available total fronthaul rate to achieve a large OSR (for the lowest value of  $R_{\text{fh}}$  considered in the figure, i.e., 21.6 Gbit/s, we have that  $O = 225$ ), rather than to densify the AP deployment.

As  $R_{\text{fh}}$  increases, the EVM decreases for each fixed  $B$ , but at different speeds: the larger  $B$ , the faster the rate of decay, in



(a) Bussgang MR/ZF combiner



(b) Bussgang LMMSE combiner

Fig. 4: EVM as a function of the fronthaul rate  $R_{\text{fh}}$ , for the case of Bussgang MR/ZF and LMMSE combiners and  $U = 1$ . The value of  $E_d$  is optimized for each value of fronthaul rate considered in the figure. The dashed lines denote the EVM for the case of infinite fronthaul rate, computed using (53) and (58), and setting  $E_d = 0$ , in accordance to the discussion in Section IV-B.

agreement with the asymptotic results in (53) and (58), which, for the channel model used in this section, predict (as illustrated in Fig. 4) that the asymptotic EVM decreases monotonically with  $B$ .

With ZF, maintaining optimality in terms of EVM requires one to progressively switch from a deployment with less APs to a deployment with more APs as the total fronthaul rate is increased. Indeed, we see that we need to switch from 4 to 16 APs when the total fronthaul rate is larger or equal to 86.4 Gbit/s and then switch again from 16 to 64 when the total fronthaul rate is larger or equal to 2764.8 Gbit/s.

The trend with LMMSE is different. Although the EVM still decays monotonically with  $R_{\text{fh}}$ , there is no penalty in setting  $B = 64$  when  $R_{\text{fh}}$  is small. Indeed, when  $R_{\text{fh}}$  is small, the EVM achieved for the three values of  $B$  considered in the figure are similar. This suggests that, in this regime, one can trade spectral oversampling with temporal oversampling.

## B. Multiple UEs

1) *Fixed UEs Positions*: We next generalize the analysis performed in Section V-A to the case of multiple UEs ( $U > 1$ ). We start by considering the scenario depicted in Fig. 2b, where  $U = 4$  UEs are deterministically placed in a square grid.

<sup>11</sup>In the remainder of the paper, the OSR corresponding to a given pair  $(B, R_{\text{fh}})$  is obtained by assuming that (6) holds with equality.

<sup>12</sup>Using [42, Eq. (1)], the expectation in (53) can be computed in closed form for the channel model considered in this section.

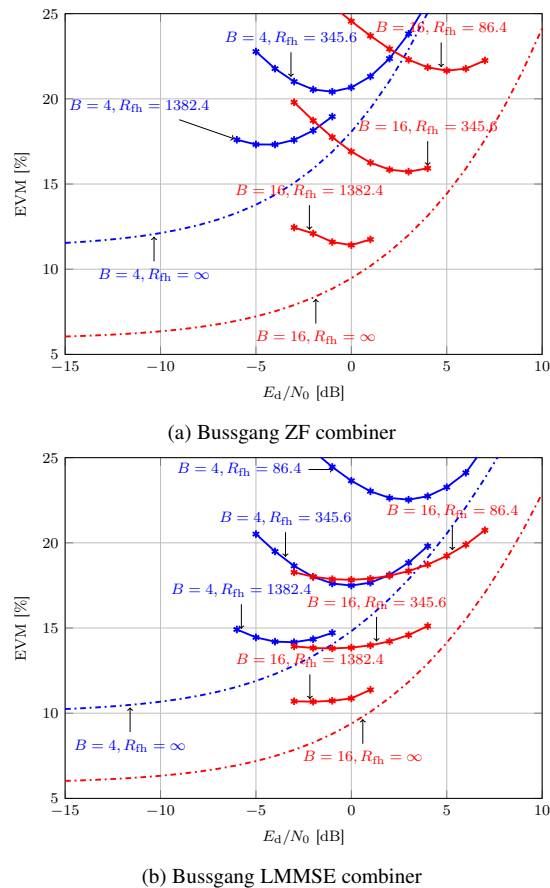


Fig. 5: EVM as a function of the dither-to-noise ratio  $E_d/N_0$ , for the case of Bussgang ZF and LMMSE combiners and  $U = 4$ . The dot-dashed lines denote the EVM for the case of infinite fronthaul rate, computed by substituting (44) and (49) into (30) and (36).

First, we verify whether the insights we reported in Section IV-B hold also for the case  $U > 1$ . In Fig. 5, we plot the EVM achievable with ZF and LMMSE combiners, computed using (30) and (36), for the same  $(B, R_{\text{fh}})$  pairs we analyzed in Fig. 3. We also plot their asymptotic limit for  $R_{\text{fh}} \rightarrow \infty$  obtained this time by substituting (44) and (49) into (30) and (36). We do not consider the MR combiner, since for the scenario considered in this section, it yields an EVM exceeding 40% for both  $B = 16$  and  $B = 4$  even in the asymptotic limit  $R_{\text{fh}} \rightarrow \infty$  and when  $E_d = 0$ . This high EVM value is caused by residual multiuser interference.

As shown in Fig. 5, the findings reported in Section IV-B still hold, namely, i) for each  $(B, R_{\text{fh}})$  pair, there exists a nonzero  $E_d/N_0$  value that minimizes the EVM; ii) for fixed  $R_{\text{fh}}$ , the asymptotic limit is approached by increasing  $E_d/N_0$  beyond the optimal value; iii) larger fronthaul values result in smaller  $E_d/N_0$ ; iv) for a given OSR, increasing  $B$  increases  $E_d/N_0$ ; v) the nonasymptotic EVM curve is flatter around its minimum with LMMSE than with ZF.

We next analyze in Fig. 6 the impact of the fronthaul rate on the EVM. Differently for the case  $U = 1$  analyzed in Fig. 4, we see that, for both Bussgang ZF and LMMSE combiners, the architecture with  $B = 64$  APs outperforms the architecture with  $B = 4$  and  $B = 16$  APs for all values of  $R_{\text{fh}}$  considered in the

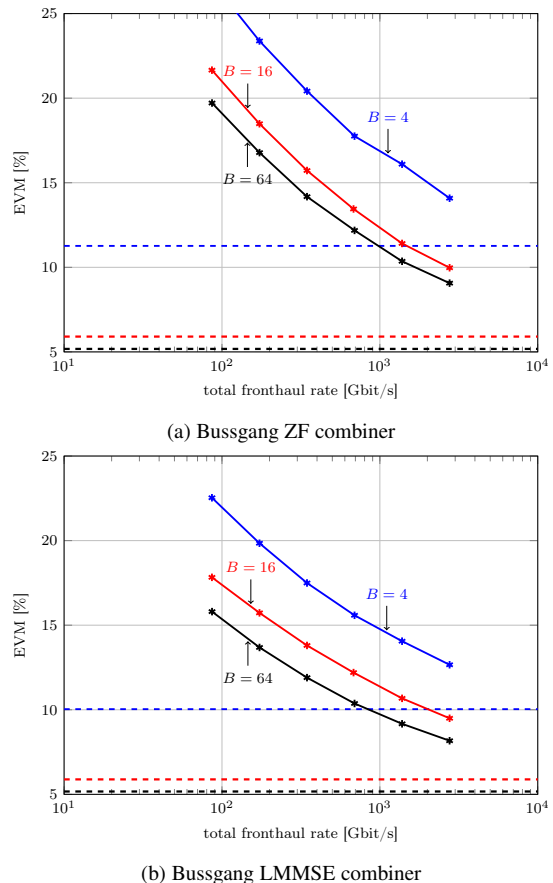


Fig. 6: EVM as a function of the fronthaul rate  $R_{\text{fh}}$ , for the case of Bussgang ZF and LMMSE combiners and  $U = 4$ . The value of  $E_d$  is optimized for each value of fronthaul rate considered in the figure. The dashed lines denote the EVM for the case of infinite fronthaul rate, computed substituting (44) and (49) into (30) and (36), and setting  $E_d = 0$ , in accordance to the discussion in Section IV-B.

figure. For the case of ZF, this means that, when  $U = 4$ , the reduction in the distance between each UE and the closest AP overcomes the deleterious effect on the EVM of a reduction in the OSR when  $R_{\text{fh}}$  is small, noticed in Fig. 4. Note also that the gap between the EVM curves and their asymptotic counterparts, computed substituting (44) and (49) into (30) and (36), and setting  $E_d = 0$ , is larger than for the  $U = 1$  case illustrated in Fig. 4, which suggests that larger fronthaul values are required to operate close to the asymptotic limits.

2) *Random UEs Positions*: We consider the situation in which four UEs are dropped independently and uniformly at random over the coverage area, while the APs are deployed over a square grid as in Fig. 2b. Focusing only on the LMMSE combiner, we report in Fig. 7 the EVM *availability*, which we define as the probability, computed with respect to the random UEs positions, that the EVM is smaller than 12.5%, as a function of the total fronthaul rate. We chose this EVM value because it is the minimum EVM required in LTE and 5G NR to support 16-QAM [43], [44]. For reference, we also illustrate the EVM achieved by a co-located massive MIMO architecture in which a BS, equipped with 64 antennas and positioned at the center of the coverage area, serves all 4 UEs. For this co-located architecture, we consider the favorable scenario of infinite fronthaul rate and no quantization (infinite precision).

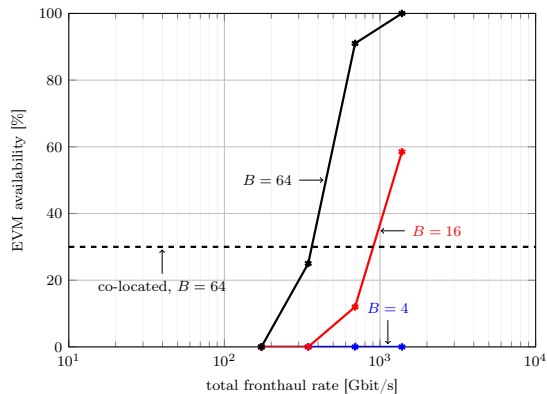


Fig. 7: EVM availability for  $U = 4$  randomly positioned UEs. The dashed line denotes the EVM availability for a co-located system in which a massive MIMO base station with 64 antennas serves all four UEs.

As illustrated in Fig. 7, an EVM availability of 100% is achieved with the 1-bit radio-over-fiber fronthaul architecture considered in this paper for the case of  $B = 64$  APs, provided that the fronthaul rate is at least 1382.4 Gbit/s. The distributed massive MIMO architecture with  $B = 64$  APs significantly outperforms the co-located massive MIMO architecture, whose EVM availability, which is 30%, is derived under the optimistic assumption of no quantization and infinite fronthaul rate. The distributed MIMO architecture with  $B = 16$  APs also outperforms the co-located architecture when the total fronthaul rate is at least 1382.4 Gbit/s. However, this architecture is not able to provide an EVM availability close to 100% for the total fronthaul rates considered in the figure. Finally, for the distributed MIMO architecture with  $B = 4$  APs, the required EVM target is not achieved for any of the random user placements considered in the simulation.

### C. Imperfect Channel Knowledge

In this section, we investigate the impact of imperfect channel knowledge on the EVM. We start by noting that the expressions for the EVM with MR and ZF combiners can be easily adapted to the case of imperfect channel knowledge. Specifically, let  $\tilde{\mathbf{H}}_k \in \mathbb{C}^{B \times U}$  be the estimate of  $\hat{\mathbf{H}}_k$  available at the receiver. Furthermore, let

$$\tilde{\mathbf{R}}_{\mathbf{q}}[0] = \frac{E_d}{2} \mathbf{I}_B + \frac{1}{N} \Re \left\{ \sum_{k \in \mathcal{S}} E_s \tilde{\mathbf{H}}_k \tilde{\mathbf{H}}_k^H + N_0 \mathbf{I}_B \right\} \quad (63)$$

and set

$$\tilde{\mathbf{G}} = \sqrt{\frac{2}{\pi}} \text{diag}(\tilde{\mathbf{R}}_{\mathbf{q}}[0])^{-1/2}. \quad (64)$$

Finally, let

$$\tilde{\mathbf{F}}_k = \left( \tilde{\mathbf{H}}_k^H \tilde{\mathbf{H}}_k \right)^{-1} \tilde{\mathbf{H}}_k^H \quad (65)$$

and

$$\mathbf{Q}_k = \tilde{\mathbf{F}}_k \tilde{\mathbf{G}}^{-1} \mathbf{G} \hat{\mathbf{H}}_k - \mathbf{I}. \quad (66)$$

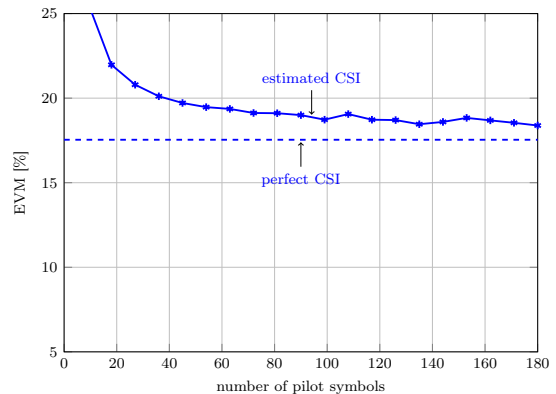


Fig. 8: EVM as a function of the number of pilot symbols:  $U = 1$ ,  $B = 4$ ,  $R_{\text{fb}} = 43.2$  Gbit/s, ZF combiner, and Bussgang LMMSE channel estimator. The dashed line denotes the EVM achievable with perfect channel state information (CSI).

Then, for the case of Bussgang ZF combiner, we have that

$$\begin{aligned} \eta^2 = & \frac{1}{E_s U S} \sum_{k \in \mathcal{S}} \left( E_s \mathbb{E} [\text{tr}(\mathbf{Q}_k \mathbf{Q}_k^H)] \right. \\ & + (N_0 + E_d) \mathbb{E} \left[ \text{tr}(\tilde{\mathbf{F}}_k \tilde{\mathbf{G}}^{-2} \mathbf{G}^2 \tilde{\mathbf{F}}_k^H) \right] \\ & \left. + \mathbb{E} \left[ \text{tr}(\tilde{\mathbf{F}}_k \tilde{\mathbf{G}}^{-1} \mathbf{C}_{\tilde{\mathbf{e}}_k} \tilde{\mathbf{G}}^{-1} \tilde{\mathbf{F}}_k^H) \right] \right). \quad (67) \end{aligned}$$

A similar expression can be obtained to the Bussgang MR combiner. One could also derive an LMMSE combiner that takes into account of the channel estimation errors. However, such a combiner admits a closed-form expression only under certain assumptions on  $\tilde{\mathbf{H}}_k$  (e.g., when it is obtained via minimum mean square error estimation, and when  $\tilde{\mathbf{H}}_k$  and  $\hat{\mathbf{H}}_k$  are jointly Gaussian—see [45, eqs. (26) and (28)]), which typically do not hold for the case of 1-bit quantization. Hence, we will not pursue this direction.

In the remainder of the section, we return to the case  $U = 1$ ,  $B = 4$ , assume that  $R_{\text{fb}} = 43.2$  Gbit/s and focus on the Bussgang LMMSE channel estimator proposed in [20]. In Fig. 8, we illustrate the EVM achievable in this scenario, computed using (67), as a function of the number of pilot symbols. We allow the power of the dither signal in the channel-estimation phase and in the data-transmission phase to be different, and optimize both values. For comparison, we also depict the EVM achievable when the channel is perfectly known to the CPU. Not surprisingly, as the number of pilot symbols increase, the EVM decreases and approaches, although slowly, the one corresponding to perfect channel knowledge. Perhaps more interesting, the optimal  $E_d/N_0$  for the pilot-transmission phase is much larger than that for the data-transmission phase (which is  $-3$  dB), and increases monotonically with the number of pilots. Specifically, it equals 5 dB when 9 pilots are transmitted, and reaches 10 dB for the case of 180 pilots. This is in agreement with the observation, reported in [46], that the normalized mean-squared error achieved by the Bussgang LMMSE channel estimator decreases as a function of the number of pilot symbols only if the SNR before quantization is decreased simultaneously.

## VI. CONCLUSIONS

We have provided a characterization of the EVM achievable in the uplink of a distributed massive MIMO architecture with 1-bit radio-over-fiber fronthaul. Our analysis allows one to characterize the impact of a fronthaul constraint on performance and to shed light on the optimal design of the dither signal and on the role of spatial and temporal oversampling in such an architecture. In particular, our numerical results illustrate that, when linear combiners are used at the CPU, and the UEs transmitted power is assumed to be inversely proportional to the number of APs, spatial oversampling is preferable to temporal oversampling for sufficiently large fronthaul rate. This is because spatial oversampling reduces multiuser interference, and, for the path-loss model considered in our simulations, yields a lower EVM, even if only a single user is active, in the limit of large fronthaul rates. However, when the fronthaul rate is small, a single user is active, and MR combiner is used, temporal oversampling may be preferable to spatial oversampling, since it results in less correlated quantization noise.

Our analysis reveals that the gains of distributed MIMO deployments over co-located deployments can be unleashed with the 1-bit radio-over-fiber fronthaul architecture considered in the paper, despite the nonlinearity introduced by the 1-bit quantization operation. In future works, we will generalize our analysis to the case in which the APs are equipped with multiple antennas, and the case in which the signal exchanged between the APs and the CPU has more than two levels. This requires an accurate modeling of the distortion occurring over the fiber-optical fronthaul.

### APPENDIX A PROOF OF LEMMA 1

To prove (45), we note that, for  $b = b'$  and  $m = 0$ , the random variable  $s_{bb'}[m]$  in (40) reduces to

$$s_{bb'}[0] = \frac{c[0](E_s \|\mathbf{h}_b\|^2 + N_0) + \frac{E_d}{2}}{p_b^2} \quad (68)$$

$$= \frac{\frac{S}{N}(E_s \|\mathbf{h}_b\|^2 + N_0) + \frac{E_d}{2}}{p_b^2} = 1. \quad (69)$$

Here, the second equality follows because  $c[0] = S$  (see (38)), and the third equality follows from the definition of  $p_b$  in (37). Next, we establish that  $s_{bb'}[m] \leq s_{bb'}[0]$ . The desired result then follows from (41), from the monotonicity of the function  $f(x) = \arcsin(x) - x$ , and because  $f(1) = \pi/2 - 1$ . Note that, when  $b \neq b'$  or  $m \neq 0$ ,

$$s_{bb'}[m] \leq \frac{\frac{S}{N} |E_s \mathbf{h}_b^T \mathbf{h}_{b'}^* + N_0|}{p_b p_{b'}} \quad (70)$$

$$\leq \frac{\frac{S}{N} (E_s \|\mathbf{h}_b\| \|\mathbf{h}_{b'}\| + N_0)}{p_b p_{b'}} \leq 1. \quad (71)$$

Here, in the first inequality we used that, for all  $x \in \mathbb{R}$ ,  $\Re\{x\} \leq |x|$ ; the second inequality is a consequence of triangle and Cauchy-Schwarz inequalities; finally, in the last inequalities we have lower-bounded the denominator and, hence, upper-

bounded the ratio, by neglecting the term  $E_d/2$  in  $p_b$  and  $p_{b'}$ ; we also used that for all nonnegative  $a, b, c$ ,

$$\frac{ab + c}{\sqrt{a^2 + c}\sqrt{b^2 + c}} \leq 1. \quad (72)$$

To establish (46), we note that, when  $b \neq b'$  or  $m \neq 0$ , we have that

$$|s_{bb'}[m]| \leq \frac{\frac{S}{N} (E_s \|\mathbf{h}_b\| \|\mathbf{h}_{b'}\| + N_0)}{p_b p_{b'}} \xrightarrow{\text{a.s.}} 0, \quad N \rightarrow \infty, \quad u = 1, \dots, B. \quad (73)$$

The last step follows because, as  $N \rightarrow \infty$ , the numerator vanishes, whereas the denominator converges to  $E_d/2$ .

To establish (47), we note that, as a consequence of (41), of the monotonicity of  $f(x)$ , and of its symmetry,

$$|r_{bb'}[m]| = |f(s_{bb'}[m])| = f(|s_{bb'}[m]|). \quad (74)$$

Also note that for  $m \geq 1$  (and also when  $m = 0$  but  $b \neq b'$ ),

$$|s_{bb'}[m]| \leq \min \left\{ 1, \frac{2S(E_s \|\mathbf{h}_b\| \|\mathbf{h}_{b'}\| + N_0)}{NE_d} \right\}. \quad (75)$$

Here, the inequality is obtained by proceeding as in (71) and then using that  $p_b \geq \sqrt{E_d/2}$ . Hence,

$$\sum_{m=1}^{N-1} |r_{bb'}[m]| \leq \sum_{m=1}^{N-1} f \left( \min \left\{ 1, \frac{2S(E_s \|\mathbf{h}_b\| \|\mathbf{h}_{b'}\| + N_0)}{NE_d} \right\} \right) \quad (76)$$

$$= Nf \left( \min \left\{ 1, \frac{2S(E_s \|\mathbf{h}_b\| \|\mathbf{h}_{b'}\| + N_0)}{NE_d} \right\} \right). \quad (77)$$

The desired result follows because

$$\lim_{N \rightarrow \infty} N^3 f(1/N) = 1/6 \quad (78)$$

from which (47) follows via (77).

### APPENDIX B PROOF OF THEOREM 2

First note that, for the case  $U = 1$ , the Bussgang MR and ZF combiners coincide. Let us first assume that we can interchange limit and expectation. Then, specializing (29) for the case of frequency-flat fading and  $U = 1$ , and using (44) and (49), we conclude that

$$\lim_{N \rightarrow \infty} \eta^2 = \frac{1}{E_s} \left( (N_0 + E_d) \mathbb{E} \left[ \frac{1}{\|\mathbf{h}\|^2} \right] + 2 \left( 1 - \frac{2}{\pi} \right) \frac{\pi E_d}{4} \mathbb{E} \left[ \frac{1}{\mathbb{E}[\|\mathbf{h}\|^2]} \right] \right), \quad (79)$$

from which (53) follows after simplifications.



To show that expectation and limit can be interchanged, we rewrite  $\eta^2$  for finite  $N$  as

$$\begin{aligned} \eta^2 &= \frac{N_0 + E_d}{E_s} \mathbb{E} \left[ \frac{1}{\|\mathbf{h}\|^2} \right] + \frac{1}{E_s} \sum_{b=1}^B \mathbb{E} \left[ \frac{2}{\|\mathbf{h}\|^4} |h_b|^2 p_b^2 r_{bb}[0] \right] \\ &+ \frac{1}{E_s} \sum_{b=1}^B \sum_{b' \neq b}^B \mathbb{E} \left[ \frac{2}{\|\mathbf{h}\|^4} h_b^* h_{b'} p_b p_{b'} r_{bb'}[0] \right] \\ &+ \frac{1}{SE_s} \sum_{m=1}^{N-1} \sum_{b=1}^B \sum_{b'=1}^B \mathbb{E} \left[ \frac{2}{\|\mathbf{h}\|^4} h_b^* h_{b'} p_b p_{b'} r_{bb'}[m] \right] \\ &\times c[m] e^{-j2\pi \frac{f_c}{f_s} m}. \end{aligned} \quad (80)$$

Next, we use the dominated convergence theorem [47, Thm. 1.34] three times, to show that the limit  $N \rightarrow \infty$  can be interchanged with the expectation in the last three terms comprising (80). Specifically, in the second term in (80), the interchange can be performed if there exists a random variable  $\gamma_b$ ,  $b \in \{1, \dots, B\}$ , not depending on  $N$  and satisfying

$$\mathbb{E} \left[ |h_b|^2 \gamma_b^2 / \|\mathbf{h}\|^4 \right] < \infty \quad (81)$$

and

$$p_b^2 \leq \gamma_b^2 \quad \text{a.s. for all } b, \text{ and } N. \quad (82)$$

To obtain this random variable, we set

$$\gamma_b = \sqrt{S(E_s |h_b|^2 + N_0) + E_b/2} \quad (83)$$

and note that  $p_b \leq \gamma_b$  for all  $N$ . Furthermore, (81) follows from (51).

In the third term in (80), the interchange can be performed if there exist random variables  $t_{bb'}$ ,  $b, b' \in \{1, \dots, B\}$  with  $b \neq b'$  not depending on  $N$  and satisfying

$$\mathbb{E} \left[ h_b^* h_{b'} t_{bb'} / \|\mathbf{h}\|^4 \right] < \infty \quad (84)$$

and

$$|p_b p_{b'} r_{bb'}[0]| \leq t_{bb'}, \quad \text{a.s.} \quad (85)$$

for all  $N$  and all  $b, b'$  with  $b \neq b'$ . To construct these random variables, we use (45) to conclude that

$$|r_{bb'}[0]| \leq \pi/2 - 1. \quad (86)$$

It follows from (86) and (82) that (85) holds with  $t_{bb'}$  given in (54). Finally, (84) follows from (51).

In the fourth term in (80), the interchange can be performed if there exist random variables  $\bar{t}_{bb'}$ ,  $b, b' \in \{1, \dots, B\}$  not depending on  $N$  and satisfying

$$\mathbb{E} \left[ \frac{h_b^* h_{b'}}{\|\mathbf{h}\|^4} \bar{t}_{bb'} \right] < \infty \quad (87)$$

and

$$\left| \sum_{m=1}^{N-1} p_b p_{b'} r_{bb'}[m] c[m] e^{-j2\pi \frac{f_c}{f_s} m} \right| \leq \bar{t}_{bb'} \quad \text{a.s. for all } b, b', N. \quad (88)$$

Proceeding as in the previous parts, we observe that

$$\begin{aligned} &\left| \sum_{m=1}^{N-1} p_b p_{b'} r_{bb'}[m] c[m] e^{-j2\pi \frac{f_c}{f_s} m} \right| \\ &\leq \gamma_b \gamma_{b'} S \sum_{m=1}^{N-1} |r_{bb'}[m]| \end{aligned} \quad (89)$$

$$\leq \gamma_b \gamma_{b'} S N f \left( \min \left\{ 1, \frac{2SE_s |h_b| |h_{b'}| + N_0}{NE_d} \right\} \right) \quad (90)$$

$$\leq \left( \frac{\pi}{2} - 1 \right) S \gamma_b \gamma_{b'} \left( \frac{2SE_s |h_b| |h_{b'}| + N_0}{E_d} \right). \quad (91)$$

Here, in the first inequality we used (82) and the triangle inequality; the second inequality follows from (77); in the third inequality, we used that the function  $f(x)/x$  is monotonically increasing in  $x$  and that  $f(x) \leq (\pi/2 - 1)x$ . It then follows from (91) that (88) holds with  $\bar{t}_{bb'}$  given in (55). Finally, (87) follows from (52).

We now prove (58). If limit and expectation can be interchanged, then (58) follows directly from (36), (44), and (49). To prove that the expectation and the limit can indeed be interchanged, we use again the dominated convergence theorem. We start by noting that, for the frequency-flat case and when  $U = 1$ , the EVM expression (36) simplifies to

$$\eta^2 = \frac{1}{S} \sum_{k \in \mathcal{S}} \mathbb{E} \left[ \frac{1}{1 + z_k} \right], \quad (92)$$

where

$$z_k = \mathbf{h}^H \left( \frac{N_0 + E_d}{E_s} \mathbf{I}_B + \frac{1}{E_s} \mathbf{G}^{-1} \mathbf{C}_{\hat{\mathbf{e}}_k} \mathbf{G}^{-1} \right)^{-1} \mathbf{h}, \quad (93)$$

with the entry on the  $b$ th row and  $b'$ th column of the matrix  $\mathbf{G}^{-1} \mathbf{C}_{\hat{\mathbf{e}}_k} \mathbf{G}^{-1}$  given by

$$\begin{aligned} \left[ \mathbf{G}^{-1} \mathbf{C}_{\hat{\mathbf{e}}_k} \mathbf{G}^{-1} \right]_{b,b'} &= \\ &2 \sum_{m=0}^{N-1} p_b p_{b'} r_{bb'}[m] e^{-j2\pi (k/N + f_c/f_s)m}, \\ &b = 1, \dots, B, b' = 1, \dots, B. \end{aligned} \quad (94)$$

We shall show that there exists a random variable  $\bar{\gamma}$  that does not depend on  $N$  and satisfies

$$\mathbb{E}[1/(1 + \bar{\gamma})] < \infty \quad (95)$$

and

$$\frac{1}{1 + z_k} \leq \frac{1}{1 + \bar{\gamma}} \quad \text{a.s. for all } N \text{ and } k \in \mathcal{S}. \quad (96)$$

Let

$$\mathbf{P}_k = \frac{N_0 + E_d}{E_s} \mathbf{I}_B + \frac{1}{E_s} \mathbf{G}^{-1} \mathbf{C}_{\hat{\mathbf{e}}_k} \mathbf{G}^{-1}. \quad (97)$$

By construction,  $\mathbf{P}_k$  is Hermitian and positive definite. As a consequence,  $\mathbf{P}_k^{-1}$  is also Hermitian and positive definite. Let  $\lambda_{\min}(\mathbf{P}_k^{-1})$  denote the smallest eigenvalue of  $\mathbf{P}_k^{-1}$ , and  $\lambda_{\max}(\mathbf{P}_k)$  denote the largest eigenvalue of  $\mathbf{P}_k$ . Note that, almost surely,

$$\mathbf{h}^H \mathbf{P}_k^{-1} \mathbf{h} \geq \lambda_{\min}(\mathbf{P}_k^{-1}) \|\mathbf{h}\|^2 = \frac{1}{\lambda_{\max}(\mathbf{P}_k)} \|\mathbf{h}\|^2 \quad (98)$$

$$\geq \frac{1}{\text{tr}(\mathbf{P}_k)} \|\mathbf{h}\|^2. \quad (99)$$

Here, the first inequality follows from the Rayleigh-Ritz Theorem [40, Thm. 4.2.2] and the second inequality follows because the trace of  $\mathbf{P}_k$  is equal to the sum of the eigenvalues of  $\mathbf{P}_k$ . Finally, note that, as a consequence of (94), (82), (85), and proceeding similarly to (89)–(91),

$$\begin{aligned} \text{tr}(\mathbf{P}_k) &= \frac{N_0 + E_d}{E_s} B \\ &+ \frac{2}{E_s} \sum_{b=1}^B \sum_{b'=1}^B \sum_{m=0}^{N-1} p_b p_{b'} \tau_{bb'} [m] e^{-j2\pi(k/N + f_c/f_s)m} \\ &\leq \frac{N_0 + E_d}{E_s} B + \frac{2}{E_s} \sum_{b=1}^B \gamma_b^2 \left( \frac{\pi}{2} - 1 \right) \\ &+ \frac{2}{E_s} \sum_{b=1}^B \sum_{b'=1}^B t_{bb'} + \frac{2}{E_s S} \sum_{b=1}^b \sum_{b'=1}^B \bar{t}_{bb'}. \end{aligned} \quad (100)$$

As a consequence, we conclude that (96) holds with  $\bar{\gamma}$  given in (57). Finally, we note that (95) coincides with assumption (56).

## REFERENCES

- [1] S. Jacobsson, L. Aabel, M. Coldrey, I. C. Sezgin, C. Fager, G. Durisi, and C. Studer, "Massive MU-MIMO-OFDM uplink with direct RF-sampling and 1-bit ADCs," in *Proc. IEEE Global Telecommun. Conf. (GLOBECOM)*, Waikoloa, HI, USA, Dec. 2019.
- [2] H. Q. Ngo, A. Ashikhmin, H. Yang, E. G. Larsson, and T. L. Marzetta, "Cell-free massive MIMO versus small cells," *IEEE Trans. Wireless Commun.*, vol. 16, no. 3, pp. 1834–1850, Mar. 2017.
- [3] E. Nayebi, A. Ashikhmin, T. L. Marzetta, H. Yang, and B. D. Rao, "Precoding and power optimization in cell-free Massive MIMO systems," *IEEE Trans. Wireless Commun.*, vol. 16, no. 7, pp. 4445–4459, Jul. 2017.
- [4] Ö. T. Demir, E. Björnson, and L. Sanguinetti, *Foundations of user centric cell-free massive MIMO*, ser. Foundations and Trends in Signal Processing, now Publishers, 2020, vol. 14, no. 3-4.
- [5] E. Björnson and L. Sanguinetti, "Making cell-free massive MIMO competitive with MMSE processing and centralized implementation," *IEEE Trans. Wireless Commun.*, vol. 19, no. 1, pp. 77–90, Jan. 2020.
- [6] J. Rodriguez Sanchez, F. Rusek, O. Edfors, M. Sarajlic, and L. Liu, "Decentralized Massive MIMO Processing Exploring Daisy-Chain Architecture and Recursive Algorithms," *IEEE Trans. Signal Process.*, vol. 68, pp. 687–700, Jan. 2020.
- [7] Z. H. Shaik, E. Björnson, and E. G. Larsson, "MMSE-optimal sequential processing for cell-free massive MIMO with radio stripes," *IEEE Trans. Commun.*, vol. 69, no. 11, pp. 7775–7789, Nov. 2021.
- [8] M. E. Rasekh, M. Abdelghany, U. Madhow, and M. Rodwell, "Phase noise in modular millimeter wave massive MIMO," *IEEE Trans. Wireless Commun.*, vol. 20, no. 10, pp. 6522–6535, Oct. 2021.
- [9] E. G. Larsson, "Massive synchrony in distributed antenna systems," *IEEE Trans. Signal Process.*, Jan. 2024, to appear.
- [10] L. Aabel, G. Durisi, I. C. Sezgin, S. Jacobsson, C. Fager, and M. Coldrey, "Distributed massive MIMO via all-digital radio over fiber," in *Proc. Asilomar Conf. Signals, Syst., Comput.*, Pacific Grove CA, U.S.A., Nov. 2020.
- [11] I. C. Sezgin, L. Aabel, S. Jacobsson, G. Durisi, Z. S. He, and C. Fager, "All-digital, radio-over-fiber, communication link architecture for time-division duplex distributed antenna system," *J. Lightw. Technol.*, vol. 39, no. 9, pp. 2769–2779, Feb. 2021.
- [12] R. F. Cordeiro, A. Prata, A. S. Oliveira, J. M. Vieira, and N. B. De Carvalho, "Agile all-digital RF transceiver implemented in FPGA," *IEEE Trans. Microw. Theory Techn.*, vol. 65, no. 11, pp. 4229–4240, Nov. 2017.
- [13] J. Wang, Z. Jia, L. A. Campos, and C. Knittle, "Delta-sigma modulation for next generation fronthaul interface," *J. Lightw. Technol.*, vol. 37, no. 12, pp. 2838–2850, Jun. 2019.
- [14] C.-Y. Wu, H. Li, O. Caytan, J. Van Kerrebrouck, L. Breyne, J. Bauwelinck, P. Demeester, and G. Torfs, "Distributed multi-user MIMO transmission using real-time Sigma-Delta-over-fiber for next generation fronthaul interface," *J. Lightw. Technol.*, vol. 38, no. 4, pp. 705–713, Feb. 2020.
- [15] C. Y. Wu, H. Li, J. Van Kerrebrouck, A. Vandierendonck, I. L. De Paula, L. Breyne, O. Caytan, S. Lemey, H. Rogier, J. Bauwelinck, P. Demeester, and G. Torfs, "Distributed antenna system using sigma-delta intermediate-frequency-over-fiber for frequency bands above 24 GHz," *J. Lightw. Technol.*, vol. 38, no. 10, pp. 2764–2772, May 2020.
- [16] L. Aabel, S. Jacobsson, M. Coldrey, F. Olofsson, G. Durisi, and C. Fager, "A TDD distributed MIMO testbed using a 1-bit radio-over-fiber fronthaul architecture," Dec. 2023.
- [17] H. Jedda, J. A. Nossek, and A. Mezghani, "Minimum BER precoding in 1-bit massive MIMO systems," in *Proc. IEEE Sensor Array and Multichannel Signal Process. Workshop (SAM)*, Rio de Janeiro, Brazil, Jul. 2016.
- [18] C. Mollén, J. Choi, E. G. Larsson, and R. W. Heath, "Uplink performance of wideband massive MIMO with one-bit ADCs," *IEEE Trans. Wireless Commun.*, vol. 16, no. 1, pp. 87–100, Jan. 2017.
- [19] S. Jacobsson, G. Durisi, M. Coldrey, U. Gustavsson, and C. Studer, "Throughput analysis of massive MIMO uplink with low-resolution ADCs," *IEEE Trans. Wireless Commun.*, vol. 16, no. 6, pp. 4038–4051, Jun. 2017.
- [20] Y. Li, C. Tao, G. Seco-Granados, A. Mezghani, A. L. Swindlehurst, and L. Liu, "Channel estimation and performance analysis of one-bit massive MIMO systems," *IEEE Trans. Signal Process.*, vol. 65, no. 15, pp. 4075–4089, Aug. 2017.
- [21] S. Jacobsson, G. Durisi, M. Coldrey, and C. Studer, "Linear precoding with low-resolution DACs for massive MU-MIMO-OFDM downlink," *IEEE Trans. Wireless Commun.*, vol. 18, no. 3, pp. 1595–1609, Mar. 2019.
- [22] Y. Zhang, M. Zhou, X. Qiao, H. Cao, and L. Yang, "On the performance of cell-free massive MIMO with low-resolution ADCs," *IEEE Access*, vol. 7, pp. 117968–117977, 2019.
- [23] X. Hu, C. Zhong, X. Chen, W. Xu, H. Lin, and Z. Zhang, "Cell-free Massive MIMO systems with low resolution ADCs," *IEEE Trans. Commun.*, vol. 67, no. 10, pp. 6844–6857, Oct. 2019.
- [24] M. Bashar, K. Cumanan, A. G. Burr, H. Q. Ngo, E. G. Larsson, and P. Xiao, "Energy efficiency of the cell-free Massive MIMO Uplink with optimal uniform quantization," *IEEE Trans. Green Commun. Netw.*, vol. 3, no. 4, pp. 971–987, Dec. 2019.
- [25] G. Femenias and F. Riera-Palou, "Fronthaul-constrained cell-free massive MIMO with low resolution ADCs," *IEEE Access*, vol. 8, pp. 116195–116215, 2020.
- [26] M. Bashar, P. Xiao, R. Tafazolli, K. Cumanan, A. G. Burr, and E. Björnson, "Limited-fronthaul cell-free massive MIMO with local MMSE receiver under Rician fading and phase shifts," *IEEE Wireless Commun. Lett.*, vol. 10, no. 9, Sep. 2021.
- [27] L. T. N. Landau, M. Dörpinghaus, R. C. de Lamare, and G. P. Fettweis, "Achievable rate with 1-bit quantization and oversampling using continuous phase modulation-based sequences," *IEEE Trans. Wireless Commun.*, vol. 17, no. 10, pp. 7080–7095, Oct. 2018.
- [28] M. Schlüter, M. Dörpinghaus, and G. P. Fettweis, "Bounds on phase, frequency, and timing synchronization in fully digital receivers with 1-bit quantization and oversampling," *IEEE Trans. Commun.*, vol. 68, no. 10, pp. 6499–6513, Oct. 2020.
- [29] J. J. Bussgang, "Crosscorrelation functions of amplitude-distorted Gaussian signals," Res. Lab. Elec., Cambridge, MA, Tech. Rep. 216, Mar. 1952.
- [30] R. Vaughan, N. Scott, and D. White, "The theory of bandpass sampling," *IEEE Trans. Signal Process.*, vol. 39, no. 9, pp. 1973–1984, Sep. 1991.
- [31] A. Lapidath, *A Foundation in Digital Communication*. Cambridge, U.K.: Cambridge Univ. Press, 2009.
- [32] S. Jacobsson, "Massive multiantenna communications with low-resolution converters," Ph.D. dissertation, Chalmers University of Technology, Gothenburg, Sweden, Aug. 2019.
- [33] S. Jacobsson, G. Durisi, M. Coldrey, and C. Studer, "On out-of-band emissions of quantized precoding in massive MU-MIMO-OFDM," in *Proc. Asilomar Conf. Signals, Syst., Comput.*, Pacific Grove CA, U.S.A., Dec. 2017.
- [34] A. K. Saxena, I. Fijalkow, and A. L. Swindlehurst, "Analysis of one-bit quantized precoding for the multiuser massive MIMO downlink," *IEEE Trans. Signal Process.*, vol. 65, no. 17, pp. 4624–4634, Sep. 2017.
- [35] J. H. Van Vleck and D. Middleton, "The spectrum of clipped noise," *Proc. IEEE*, vol. 54, no. 1, pp. 2–19, Jan. 1966.
- [36] E. Björnson, L. Sanguinetti, and J. Hoydis, "Hardware distortion correlation has negligible impact on UL massive MIMO spectral efficiency," *IEEE Trans. Commun.*, vol. 67, no. 2, pp. 1085–1098, Feb. 2019.
- [37] N. Kolomvakis, T. Eriksson, M. Coldrey, and M. Viberg, "Quantized uplink massive MIMO systems with linear receivers," in *Proc. IEEE Int. Conf. Commun. (ICC)*, Jun. 2020.
- [38] L. V. Nguyen, A. L. Swindlehurst, and D. H. N. Nguyen, "Linear and deep neural network-based receivers for massive MIMO systems with one-bit

- ADCs,” *IEEE Trans. Wireless Commun.*, vol. 20, no. 11, pp. 7333–7345, Nov. 2021.
- [39] S. Jacobsson, Y. Etefagh, G. Durisi, and C. Studer, “All-digital massive MIMO with a fronthaul constraint,” in *Proc. IEEE Statistical Sig. Pro. Workshop*, Friburg, Germany, Jun. 2018.
- [40] R. A. Horn and C. R. Johnson, *Matrix Analysis*. Cambridge, U.K.: Cambridge Univ. Press, 1985.
- [41] T. Koch and A. Lapidoth, “At low SNR, asymmetric quantizers are better,” *IEEE Trans. Inf. Theory*, vol. 59, no. 9, pp. 5421–5445, Sep. 2013.
- [42] N. Cressie, A. S. Davis, J. L. Folks, and G. E. Policello, “The moment-generating function and negative integer moments,” *The American Statistician*, vol. 35, no. 3, pp. 148–150, Aug. 1981.
- [43] 3GPP, “Evolved universal terrestrial radio access (E-UTRA); base station (BS) radio transmission and reception,” 2022, TS 36.104 version 17.7.0 Rel. 17.
- [44] —, “NR; base station (BS) radio transmission and reception,” 2022, TS 38.104 version 17.7.0 Rel. 17.
- [45] A. Lapidoth and S. Shamai (Shitz), “Fading channels: How perfect need ‘perfect side information’ be?” *IEEE Trans. Inf. Theory*, vol. 48, no. 5, pp. 1118–1134, May 2002.
- [46] Y. Etefagh, A. Hu, S. Jacobsson, G. Durisi, and C. Studer, “All-digital massive MIMO uplink and downlink rates under a fronthaul constraint,” in *Proc. Asilomar Conf. Signals, Syst., Comput.*, Pacific Grove CA, U.S.A., Nov. 2019.
- [47] W. Rudin, *Real and Complex Analysis*, 3rd ed. New York, NY, U.S.A.: McGraw-Hill, 1987.